Shapes From Echoes: Uniqueness From Point-to-Plane Distance Matrices

Miranda Kreković, *Student Member, IEEE*, Ivan Dokmanić, *Member, IEEE*, and Martin Vetterli, *Fellow, IEEE*

***Abstract*—We study the problem of localizing a configuration of points and planes from the collection of point-to-plane distances. This problem models simultaneous localization and mapping from acoustic echoes as well as the "structure from sound" approach to microphone localization with unknown sources. In our earlier work we proposed computational methods for localization from point-to-plane distances and noted that such localization suffers from various ambiguities beyond the usual rigid body motions; in this paper we provide a complete characterization of uniqueness. We enumerate all cases of configurations which lead to the same distance measurements as a function of the number of planes and points, and algebraically characterize the related transformations in both 2D and 3D.**

***Index Terms*—Point-to-plane distance matrix, inverse problem in the Euclidean space, uniqueness of the reconstruction, collocated source and receiver, indoor localization and mapping.**

I. Introduction

LOCALIZATION methods are traditionally based on geometric information (angles, distances, or both) about known objects, often referred to as landmarks or anchors. Famous examples include global positioning by measuring distances to satellites and navigation at sea by measuring angles of celestial bodies. More recent work on simultaneous localization and mapping (SLAM) addresses the case where the positions of landmarks are also unknown.

In this paper, we address localization from distances to (unknown) planes instead of the more extensively studied localization from distances to points. Concretely, given pairwise distances between a set of points and a set of planes, we wish to localize both the planes and the points. It is clear that a single point does not allow unique localization. As we will show, localization is in general possible with multiple points, but there are curious exceptions.

Manuscript received February 19, 2019; revised September 6, 2019 and November 18, 2019; accepted February 24, 2020. Date of publication March 23, 2020; date of current version April 28, 2020. The associate editor coordinating the review of this manuscript and approving it for publication was Prof. Mark A. Davenport. This work was supported by the Swiss National Science Foundation under Grant 20FP-1 151073, "Inverse Problems regularized by Sparsity". The work of I. Dokmanić was supported by a Google Faculty Research Award. *(Corresponding author: Miranda Kreković.)*

Miranda Kreković and Martin Vetterli are with the School of Computer and Communication Sciences, Ecole Polytechnique Fédérale de Lausanne, CH-1015 Lausanne, Switzerland (e-mail: miranda.krekovic@epfl.ch; martin@vetterli@epfl.ch).

Ivan Dokmanić is with the Coordinated Science Laboratory, University of Illinois at Urbana-Champaign, Urbana, IL 61801 USA (e-mail: dokmanic@illinois.edu).

Digital Object Identifier 10.1109/TSP.2020.2982780

Localization from point-to-plane distances models many practical problems. Our motivation comes from indoor localization with sound. Imagine a mobile device equipped with a single omnidirectional source and a single omnidirectional receiver that measures its distance to the surrounding reflectors, for example by emitting acoustic pulses and receiving echoes. The times of flight of the first-order echoes recorded by the device correspond to point-to-plane distances. They could be used to pinpoint its location given the positions of the walls, but the problem is harder and more interesting when we do not know where the walls are. A similar principle is used by bats to echolocate, although we do not assume having any directional information. Another problem that can be cast in this mold is the well-known "structure from sound" [1], where the task is to localize a set of microphones from phase differences induced by a set of unknown far field sources.

In this work, we focus on uniqueness of reconstruction from point-to-plane distance matrices (PPDMs). Unlike in the case of localization from points, where with sufficiently many points the only possible ambiguities are those of translation, rotation, and reflection [2], our analysis shows that localization from PPDMs exhibits additional ambiguities that correspond to certain continuous deformations of the points–planes system.

A. Related Work

The PPDM problem is related to the more standard multidimensional unfolding [3]: localization of a set of points from distances to a set of point landmarks. There are several variations of this problem that correspond to different assumptions on what is known: 1) given distances to known landmarks, localize unknown points (i.e., estimate the unknown trajectory), 2) given distances to known points, reconstruct unknown landmarks (i.e., map the unknown environment), 3) estimate both unknown landmarks and unknown points from their pairwise distances.

The first variation is solved by simple multilateration when the association between the landmarks and the received signals is known [4]. When the association is unknown, it must be inferred jointly with the positions [5]. The second scenario is a topic of active research in signal processing and room acoustics, where it is known as "hearing the shape of a room" [6]–[8]. Much of that work assumes that the geometry of the microphone array is known. Then, since the source is fixed, the landmarks are modeled by points that correspond to virtual sources. In the third scenario, when neither the landmarks nor the points are known, we deal with an instance of SLAM. In general SLAM, the task is to simultaneously build some representation of the map of the environment and estimate the trajectory. Different flavors of SLAM involve different sensing modalities, but our interest is primarily in SLAM from reflections of sound or

radio waves from walls, as well as solutions based on multiple sensor modalities that provide range measurements [9]–[12]. In this context, the "map" consists of the positions of the planar reflectors.

The existing related literature can be broadly categorized into three groups. In the first group, a mobile robot is equipped with a microphone array or multimodal sensors, and aims to localize multiple interfering sound sources inside a reverberant environment [13]–[17]. Such methods often require high-end equipment [12] or precise calibration of microphone positions in the array, sometimes combined with beamforming [13], [14].

The second group involves more recent works that rely on simpler mobile devices equipped with either a source or a receiver [18]–[24]. To recover rooms, the devices leverage multipath wave propagation from static anchors, and the fact that the echoes correspond to range measurements from *virtual* anchors. Combined with Bayesian techniques such as belief propagation that jointly perform data association and estimate the state of the mobile agent and the environment, this can lead to robust SLAM [24]; beyond timing, valuable information is contained in the amplitude statistics of the multipath components [25], [26]. In [27], the authors present a setup in which the mobile agent is a commodity smartphone acting as a receiver, while the source is fixed at an unknown location; their approach handles unlabeled, missing and spurious echoes in realistic environments.

The third group, which we address here, comprises setups with no fixed beacons inside rooms, and a mobile robot capable of only rudimentary sensing. This group has received the least attention, but it is appealing from a cost and technological perspective. Moreover, it overcomes the drawbacks associated with the second group, where the reconstruction accuracy depends not only on the receiver's trajectory, but also on the position of the static anchors. The authors in [28] and [29] propose to reconstruct the geometry of walls from short-range room scans obtained by a sound source and two microphones on a smartphone. The short-range scans reveal distances between the smartphone and the nearby walls. In [30], the authors present a biomimetic sonar with one emitter and two receivers. They rely on the echolocation-related transfer function (ERTF) to estimate the angles of arrival of echoes, and compute the distances between the sonar and the walls from the measured propagation times of echoes.

As evident from the above discussion, prior work on indoor localization from audio and radio waves mostly focuses on computational aspects. However, more recent research in the context of 5G multipath-based positioning and mapping leverages geometry-based stochastic model of the received signal to derive theoretical position error bounds [31]–[34]. In [33], the authors derive the Cramér-Rao bound on the estimation uncertainty for the receiver position and orientation using a single transmitter in a multiple-input-multiple-output (MIMO) system. Moreover, the results in [34] show that one can reconstruct the state of the agent (pose, orientation and time synchronization) and the geometry of a room from at least three non-line-of-sight multipath components.

In the context of localization and mapping from point-to-plane distances, prior studies have also been primarily computational [35]–[37]. An exception is [38], where the authors consider a setup like ours and show that the uniqueness of the mapping between the first-order echoes and the room geometry is guaranteed for all polygons except parallelograms. A related uniqueness question is addressed in [39]. The authors show that one can reconstruct a room from the first-order echoes from one omnidirectional speaker to four non-planar microphones, located on a drone with generic position and orientation. Lastly, we point out problems with uniqueness in our conference papers [40], [41], but a complete study was up to now absent.

B. Our Contributions

An appeal of our setup with a collocated source and receiver, is that it does not require any preinstalled infrastructure. Unlike many other methods, localization from PPDMs corresponds to range-only SLAM, as the omni-directionality assumption prevents us from having any knowledge about the angles of arrival of echoes. Moreover, conventional approaches to SLAM rely on some noisy estimate of the trajectory, which is not assumed to be available in our setup. We also do not assume any motion model and allow for arbitrary configurations of waypoints.

We study uniqueness of reconstruction of points–planes configurations from their pairwise distances. We derive conditions under which the localization is unique, and provide a complete characterization of non-uniqueness by enumerating the cases of configurations that lead to same PPDMs. Since we are motivated by SLAM, we refer to points–planes configurations as *rooms* and *trajectories*. The conclusions, however, are general, and can be applied to any of the discussed applications.

Finally, while PPDMs provide a good basic model for SLAM from echoes with a collocated source and receiver, the full SLAM presents a number of additional challenges. Our results are relevant for any modality which allows one to measure distances to walls, be it light, radio, or sound. We do not address the various modality- or application-specific details and measurement techniques. In the acoustic case, problems of associating echoes to walls [42], dealing with missing and false positive echoes [24], [25], and distinguishing first-order from higher-order echoes will be addressed in a companion paper. Here we assume having a full PPDM as defined in Section II.

We begin by specifying the problem setup in Section II. A general study of uniqueness is given in Section III, followed by the detailed analyses of the 2D and 3D case in Sections IV and V. In Section VI we discuss implications of our results for applications and explain how geometric priors can help stabilize the problem. These strategies are thoroughly tested in computer experiments in Section VII.

II. Problem Setup

Suppose a mobile device carrying an omnidirectional source and an omnidirectional receiver traverses a trajectory described by N waypoints $\{\mathbf{r}_n\}_{n=1}^N$. At every waypoint, the source produces a pulse, and the receiver registers the echoes. In a collocated setup the propagation times of the first-order echoes give the distances between the waypoints and walls. The distance d_{nk} between the nth waypoint and the kth wall is given by

$$d_{nk} = \tfrac{1}{2} c\tau_{nk}, \tag{1}$$

where c is the speed of sound and τ_{nk} is the propagation time of the first-order echo.

To describe a room, we consider K walls $\{\mathcal{P}_k\}_{k=1}^K$ (lines in 2D and planes in 3D) defined by their unit normals $\mathbf{n}_k \in \mathbb{R}^m$ and distances from the origin $q_k \in \mathbf{R}$, $\mathcal{P}_k = (\mathbf{n}_k, q_k)$. Here $m \in \{2, 3\}$ denotes the dimension of the space. For any $\mathbf{x} \in \mathcal{P}_k$ we have $\langle \mathbf{n}_k, \mathbf{x} \rangle = q_k$. We illustrate the setup in Fig. 1.

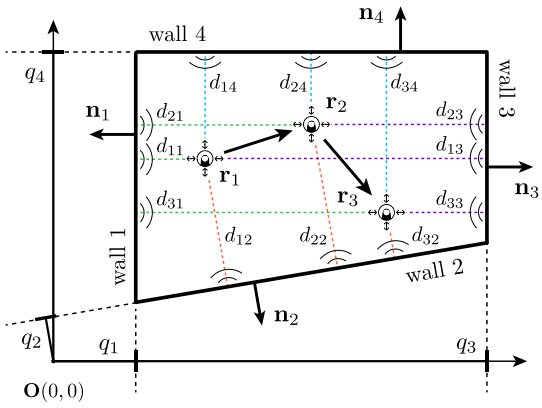

Fig. 1. Illustration of $N = 3$ points $\{\mathbf{r}_n\}_{n=1}^N$ and $K = 4$ walls $\{\mathcal{P}_k\}_{k=1}^K$ with the corresponding PPDM.

Given the distances between walls and waypoints,

$$d_{nk} = \operatorname{dist}(\mathbf{r}_n, \mathcal{P}_k) = q_k - \langle \mathbf{r}_n, \mathbf{n}_k \rangle, \tag{2}$$

for $n = 1, \ldots, N$ and $k = 1, \ldots, K$, we define

$$\mathbf{D} \stackrel{\text{def}}{=} [d_{nk}]_{n,k=1}^{N,K} \in \mathbb{R}^{N \times K} \tag{3}$$

to be the *point-to-plane distance matrix* (PPDM); we always assume $N \geq K$.

By setting $\mathbf{q} \stackrel{\text{def}}{=} [q_1, \ldots, q_K]^\top$, $\mathbf{R} \stackrel{\text{def}}{=} [\mathbf{r}_1, \ldots, \mathbf{r}_N]$, and $\mathbf{N} \stackrel{\text{def}}{=} [\mathbf{n}_1, \ldots, \mathbf{n}_K]$, we can express a PPDM as

$$\mathbf{D} = \mathbf{1}\mathbf{q}^\top - \mathbf{R}^\top \mathbf{N}, \tag{4}$$

where $\mathbf{q}$ is the vector of distances between the planes and the origin, columns of $\mathbf{R} \in \mathbb{R}^{m \times N}$ are the waypoint coordinates, and columns of $\mathbf{N} \in \mathbb{R}^{m \times K}$ outward looking normal vectors of the planes.

A pair of planes and waypoints defines a *room–trajectory* configuration $\mathcal{R} = (\{\mathcal{P}_k\}_{k=1}^K, \{\mathbf{r}_n\}_{n=1}^N)$, and the corresponding PPDM $\mathbf{D}(\mathcal{R})$. In realistic convex configurations, all entries of the PPDM (4) are non-negative. However, in our generalized definition of a room, the waypoints can lie on either side of a wall, so we allow for signed distances.

Our central question is whether a given PPDM $\mathbf{D}(\mathcal{R})$ specifies a unique room–trajectory configuration $\mathcal{R}$, or, equivalently, whether the map $\mathcal{R} \mapsto \mathbf{D}(\mathcal{R})$ is injective. It is clear that rotated, translated, and reflected versions of $\mathcal{R}$ all give the same $\mathbf{D}$, so we consider them to be the same configuration. In fact, we translate all configurations $\mathcal{R}$ by $-\mathbf{r}_1$, and thus assume $\mathbf{r}_1 = 0$ without loss of generality. As we will see later, this simplifies the analysis.

We formalize the uniqueness question as follows:

Problem 1: Are there distinct room–trajectory configurations $\mathcal{R}^1 = (\{\mathcal{P}_k^1\}_{k=1}^K, \{\mathbf{r}_n^1\}_{n=1}^N)$ and $\mathcal{R}^2 = (\{\mathcal{P}_k^2\}_{k=1}^K, \{\mathbf{r}_n^2\}_{n=1}^N)$ which are not rotated, translated, and reflected versions of each other, such that $\mathbf{D}(\mathcal{R}^1) = \mathbf{D}(\mathcal{R}^2)$?

III. Uniqueness of the Reconstruction

Perhaps surprisingly, there are many examples of rooms from Problem 1. The main tool in identifying the sought cases of room–trajectory configurations with the same PPDMs is the following lemma.

Lemma 1 (Non-uniqueness criterion): Two room–trajectory configurations $\mathcal{R}^0 = (\{\mathcal{P}_k^0\}_{k=1}^K, \{\mathbf{r}_n^0\}_{n=1}^N)$ and $\mathcal{R} = (\{\mathcal{P}_k\}_{k=1}^K, \{\mathbf{r}_n\}_{n=1}^N)$ have the same distance measurements, $\mathbf{D}(\mathcal{R}^0) = \mathbf{D}(\mathcal{R})$, if and only if

$$\bar{\mathbf{R}}^\top \bar{\mathbf{N}} = \mathbf{0}, \tag{6}$$

where

$$\bar{\mathbf{R}} \stackrel{\text{def}}{=} \begin{bmatrix} \mathbf{R}^0 \\ -\bar{\mathbf{R}} \end{bmatrix} = \begin{bmatrix} \mathbf{r}_1^0 & \ldots & \mathbf{r}_N^0 \\ -\mathbf{r}_1 & \ldots & -\mathbf{r}_N \end{bmatrix}, \tag{7}$$

$$\bar{\mathbf{N}} \stackrel{\text{def}}{=} \begin{bmatrix} \mathbf{N}^0 \\ \mathbf{N} \end{bmatrix} = \begin{bmatrix} \mathbf{n}_1^0 & \ldots & \mathbf{n}_K^0 \\ \mathbf{n}_1 & \ldots & \mathbf{n}_K \end{bmatrix}, \tag{8}$$

and the translation of $\mathcal{R}$ and $\mathcal{R}^0$ is such that $\mathbf{r}_1 = \mathbf{r}_1^0 = \mathbf{0}$.

Proof: $\mathcal{R}^0$ and $\mathcal{R}$ have the same PPDM if and only if for every $1 \leq k \leq K$ and $1 \leq n \leq N$,

$$\begin{aligned} & d_{nk}^0 = d_{nk} \\ \iff & q_k^0 - (\mathbf{r}_n^0)^\top \mathbf{n}_k^0 = q_k - \mathbf{r}_n^\top \mathbf{n}_k. \end{aligned}$$

The fact that $\mathbf{r}_1^0 = \mathbf{r}_1 = \mathbf{0}$ for $n = 1$ implies that $q_k^0 = q_k$ for every $1 \leq k \leq K$. Thus, in the matrix form we have,

$$\begin{aligned} & \mathbf{D}(\mathcal{R}^0) = \mathbf{D}(\mathcal{R}) \\ \iff & (\mathbf{R}^0)^\top \mathbf{N}^0 - \mathbf{R}^\top \mathbf{N} = 0 \\ \iff & \begin{bmatrix} \mathbf{R}^0 \\ -\mathbf{R} \end{bmatrix}^\top \begin{bmatrix} \mathbf{N}^0 \\ \mathbf{N} \end{bmatrix} = 0. \end{aligned}$$

■

From (6), it follows that given a PPDM $\mathbf{D}(\mathcal{R}^0)$, both $\mathcal{R}^0$ and $\mathcal{R}$ are valid solutions to the problem of reconstructing rooms and

$$\bar{\mathbf{N}}_{2D}^\top = \begin{bmatrix} \cos\varphi_1^0 & \sin\varphi_1^0 & \cos\varphi_1 & \sin\varphi_1 \\ \cos\varphi_2^0 & \sin\varphi_2^0 & \cos\varphi_2 & \sin\varphi_2 \\ \vdots & \vdots & \vdots & \vdots \\ \cos\varphi_K^0 & \sin\varphi_K^0 & \cos\varphi_K & \sin\varphi_K \end{bmatrix},$$

$$\bar{\mathbf{N}}_{3D}^\top = \begin{bmatrix} \sin\theta_1^0\cos\varphi_1^0 & \sin\theta_1^0\sin\varphi_1^0 & \cos\theta_1^0 & \sin\theta_1\cos\varphi_1 & \sin\theta_1\sin\varphi_1 & \cos\theta_1 \\ \sin\theta_2^0\cos\varphi_2^0 & \sin\theta_2^0\sin\varphi_2^0 & \cos\theta_2^0 & \sin\theta_2\cos\varphi_2 & \sin\theta_2\sin\varphi_2 & \cos\theta_2 \\ \vdots & \vdots & \vdots & \vdots & \vdots & \vdots \\ \sin\theta_K^0\cos\varphi_K^0 & \sin\theta_K^0\sin\varphi_K^0 & \cos\theta_K^0 & \sin\theta_K\cos\varphi_K & \sin\theta_K\sin\varphi_K & \cos\theta_K \end{bmatrix} \tag{5}$$

trajectories from PPDMs. In other words, $\mathcal{R}^0$ and $\mathcal{R}$ belong to the set of room–trajectory configurations with the same PPDMs, which we define as

$$\left[\mathcal{R}^0\right] \stackrel{\text{def}}{=} \left\{\mathcal{R} \in \mathcal{T} \;\middle|\; \mathbf{D}(\mathcal{R}) = \mathbf{D}(\mathcal{R}^0)\right\}. \tag{9}$$

Here, $\mathcal{R}^0$ is a generator of the set and $\mathcal{T}$ is a collection of all room–trajectory configurations $(\{\mathcal{P}_k\}_{k=1}^K, \{\mathbf{r}_n\}_{n=1}^N)$, such that $\mathbf{n}_k \in \mathbb{R}^m$ with $\mathbf{n}_k^\top \mathbf{n}_k = 1$, $q_k \in \mathbb{R}$, and $\mathbf{r}_n \in \mathbb{R}^m$ for $1 \le k \le K$, $1 \le n \le N$. From (9) and Lemma 1, it further follows that the set of room–trajectory configurations with the same PPDMs can be specified as:

$$\left[\mathcal{R}^0\right] = \left\{\mathcal{R} \in \mathcal{T} \;\middle|\; \bar{\mathbf{R}}^\top \bar{\mathbf{N}} = \mathbf{0}\right\}, \tag{10}$$

where $\bar{\mathbf{R}}$ contains the coordinates of the waypoints of the two equivalent rooms $\mathcal{R}^0$ and $\mathcal{R}$, while the columns of $\bar{\mathbf{N}}$ are the wall normals of $\mathcal{R}^0$ and $\mathcal{R}$; they are given in (7) and (8), respectively.

We now characterize the sets (10) by analyzing $\bar{\mathbf{R}}^\top \bar{\mathbf{N}} = \mathbf{0}$. This relation is satisfied when the columns of $\bar{\mathbf{R}}$ are in the nullspace of $\bar{\mathbf{N}}^\top$. We parameterize the unit-norm columns of $\bar{\mathbf{N}}^\top = \begin{bmatrix}\mathbf{N}^{0\top} & \mathbf{N}^\top\end{bmatrix}$ as

$$\mathbf{n}_k^0 = \begin{bmatrix}\cos\varphi_k^0 \\ \sin\varphi_k^0\end{bmatrix} \quad \text{and} \quad \mathbf{n}_k = \begin{bmatrix}\cos\varphi_k \\ \sin\varphi_k\end{bmatrix} \tag{11}$$

in 2D, and

$$\mathbf{n}_k^0 = \begin{bmatrix}\sin\theta_k^0\cos\varphi_k^0 \\ \sin\theta_k^0\sin\varphi_k^0 \\ \cos\theta_k^0\end{bmatrix} \quad \text{and} \quad \mathbf{n}_k = \begin{bmatrix}\sin\theta_k\cos\varphi_k \\ \sin\theta_k\sin\varphi_k \\ \cos\theta_k\end{bmatrix} \tag{12}$$

in 3D; $\bar{\mathbf{N}}^\top$ is written out in (5) shown at bottom of the previous page. The wall normals $\mathbf{N}^0$ and $\mathbf{N}$ of the two room–trajectory configurations $\mathcal{R}^0$ and $\mathcal{R}$ are uniquely determined by the angles $\{\varphi_k^0\}_{k=1}^K$ and $\{\varphi_k\}_{k=1}^K$ in 2D, or by the pairs of angles $\{\theta_k^0, \varphi_k^0\}_{k=1}^K$ and $\{\theta_k, \varphi_k\}_{k=1}^K$ in 3D, where $\varphi_k^0, \varphi_k \in [0, 2\pi)$ and $\theta_k^0, \theta_k \in [0, \pi)$. As the converse is also true—the matrix $\bar{\mathbf{N}}$ uniquely determines the angles—we interchangeably use both notations.

To find the configurations that are not uniquely determined by PPDMs, we impose linear dependencies among the columns of $\bar{\mathbf{N}}^\top$: we select any r linearly independent columns of $\bar{\mathbf{N}}^\top$ and assume that the remaining columns are their linear combinations. Restricting the analysis to a particular column selection does not reduce generality, as shown in Appendix.

In addition to these linear dependencies, the columns in (5) are also subject to non-linear relationships due to the normalization constraint. Indeed, $\bar{\mathbf{N}}^\top$ has K rows, $2\,m$ columns, and only $2(m-1)K$ free parameters. The combination of these linear and non-linear dependencies determines the sets of the rooms and trajectories with the same PPDMs. Our goal is to characterize these sets.

Specifically, for every set we want to find a reference configuration $\mathcal{R}^0$ that identifies the set, and a rule that generates other $\mathcal{R}$ with the same PPDM. Letting $r = \operatorname{rank}(\bar{\mathbf{N}})$, the analysis is performed for every $r \in \{1, \ldots, 2\,m-1\}$ in six steps. We introduce and explain those steps on the case $r = 2$ in 2D, rather than $r = 1$ which gives degenerate solutions (we analyze $r = 1$ subsequently).

As we will see, most of the identified cases correspond to rooms that are in some sense degenerate (for example, a "room" with all walls parallel), although as points–planes configurations they are perfectly reasonable.

The analysis in Section IV and Section V together with the fact that Lemma 1 is sufficient and necessary prove that the union of all sets described in this paper (see Fig. 2) is in fact the set of all possible configurations that are not uniquely determined by their PPDM. In other words, a room can be uniquely reconstructed from a PPDM (modulo rigid motions) if and only if it does not belong to one of the cases illustrated in Fig. 2.

Theorem 1: In 2D, a room–trajectory configuration is not uniquely determined by its PPDM, modulo rigid transformations, if and only if at least one of the following holds: 1) waypoints are collinear, 2) all walls are parallel (infinitely long corridors), 3) walls form a parallelogram possibly extended by parallel walls (see Fig. 2). In 3D, a room–trajectory configuration is not uniquely determined by its PPDM, modulo rigid transformations, if and only if at least one of the following holds: 1) $K < 6$, 2) waypoints are coplanar, 3) the configuration is in one of the cases summarized in Fig. 2.

IV. Classification of 2D Configurations

We begin by the easier 2D analysis, i.e. $m = 2$. For $\bar{\mathbf{N}}^\top$ to have a nullspace, we must have $r \in \{1, 2, 3\}$. For all r the analysis is performed as a sequence of six steps, which we describe in detail for $r = 2$.

A. 2D Rank-2: Parallelogram Rooms

1) *Linear dependence:* We select r linearly independent columns of $\bar{\mathbf{N}}^\top$, denoted $\mathbf{c}_i \in \mathbb{R}^K$, $i = 1, \ldots, r$, and denote the remaining columns of $\bar{\mathbf{N}}^\top$ by $\mathbf{c}_k \in \mathbb{R}^K$, $k = r+1, \ldots, 2\,m$. We let $\mathbf{c}_k$ for $k > r$ be linear combinations of $\mathbf{c}_k$ for $k \le r$:

$$\begin{bmatrix}\mathbf{c}_{r+1} & \ldots & \mathbf{c}_2\; m\end{bmatrix}^\top = \mathbf{T}\begin{bmatrix}\mathbf{c}_1 & \ldots & \mathbf{c}_r\end{bmatrix}^\top, \tag{13}$$

for some $\mathbf{T} \in \mathbb{R}^{(2m-r)\times r}$.

Concretely, for $r = 2$, we assume that the first two columns of $\bar{\mathbf{N}}^\top$ are linearly independent, while the third and the fourth column are their linear combinations. We prove in Appendix that this particular choice of columns does not incur a loss of generality in this or any of the other cases. From (5), for every k we have that

$$\begin{bmatrix}\cos\varphi_k \\ \sin\varphi_k\end{bmatrix} = \mathbf{T}\begin{bmatrix}\cos\varphi_k^0 \\ \sin\varphi_k^0\end{bmatrix}, \text{ where } \mathbf{T} = \begin{bmatrix}a & b \\ c & d\end{bmatrix}. \tag{14}$$

2) *Reparametrization:* When $r \le m$, we can rearrange the columns so that the right-hand side of (13) contains the normals of the reference configuration $\mathcal{R}^0$, while the left-hand side has the normals of the putative equivalent configuration $\mathcal{R}$. In particular, we obtain

$$\mathbf{N}^\top = \mathbf{T}'\mathbf{N}^{0\top}, \tag{15}$$

where $\mathbf{T}' \in \mathbb{R}^{m\times m}$. $\mathbf{T}'$ can be decomposed as a product $\mathbf{T}' = \mathbf{Q}\mathbf{U}$ of an orthogonal matrix $\mathbf{Q}$ and an upper triangular matrix $\mathbf{U}$. $\mathbf{Q}$ acts as a rotation and a reflection, so without loss of generality we set $\mathbf{Q} = \mathbf{I}$ and $\mathbf{T}' = \mathbf{U}$. That is, we assume that the entries of $\mathbf{T}'$ below the diagonal are 0, which removes the rotational degrees of freedom. Since (15) contains a subset of equations from (13), we propagate this change back to (13) by modifying the corresponding elements of $\mathbf{T}$.

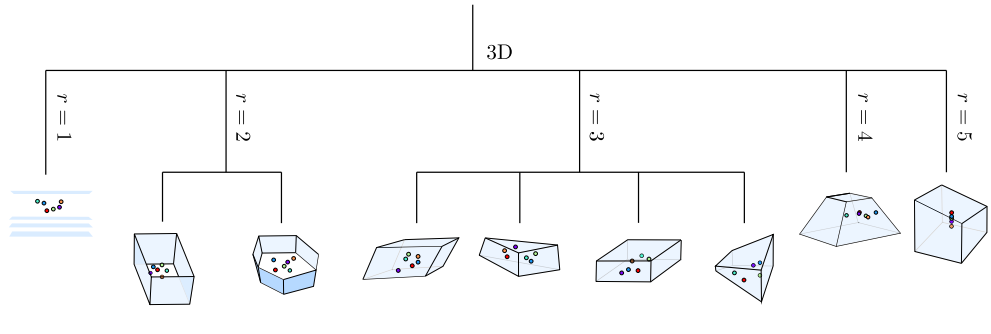

		(48)	(60)	(60), cstr: (61)		(78)	(78)	(83)	(91)	(97)
class generator	room	φ_k^0: (44) θ_k^0: (45) all walls parallel	φ_k^0: (56) θ_k^0: (53) 2 pair of parallel walls	φ_k^0 : any θ_k^0 : (53) cstr: (61) all walls parallel to a line	φ_k^0: any θ_k^0: (72)	φ_k^0: any θ_k^0: any $K_0 < 6$ any with less than 6 walls	φ_k^0: any θ_k^0: any $K_0 < 6$	$\varphi_{1,2}^0$: any θ_k^0: any two sets of parallel walls	φ_k^0: any θ_k^0: any	φ_k^0: any θ_k^0: any
	trajectory	any	any	any	any	any	any	any	planar	linear
transformation	room	none	φ_k: (57) θ_k: (57)	none	φ_k: (75) θ_k: (75)	φ_k: (75) θ_k: (75)	φ_k: (75) θ_k: (75)	φ_k: (75) θ_k: (75)	φ_k: (86) θ_k: (86)	φ_k : any θ_k: (93)
	trajectory	(47) move points in a plane	(59)	(59), cstr: (61) move points on a line parallel to the walls	(77)	(77)	(77)	(77)	(90)	(96) scale

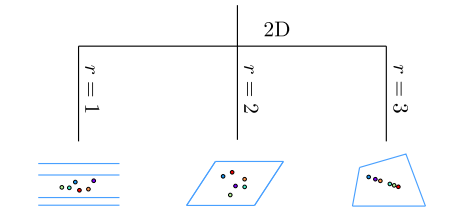

		(33)	(25)	(40)
class generator	room	φ_k^0: (30) all walls parallel	φ_k^0: (21) parallelograms	φ_k^0: any
	trajectory	any	any	linear
transformation	room	none	φ_k: (22)	φ_k: (35)
	trajectory	(32) move points on a line	(23) scale and shear	(37) scale

Fig. 2. An overview of the sets of the room–trajectory configurations with respect to PPDMs in 2D and 3D. The first row references the set-defining equation; determines the case. The middle part characterizes the set generator (wall orientations in the reference room in the grey box; information about the corresponding trajectories in the white box). The bottom part describes transformations of the reference to equivalent walls and waypoints and references corresponding equations; "cstr" indicates additional constraints on $\mathbf{T}$. Where appropriate, we provide a short description of the transformation.

When $r = m$, the original system of equations (14) already has a form of (15). Therefore, we only need to set $c = 0$ and obtain an upper triangular matrix,

$$\mathbf{T} = \begin{bmatrix} a & b \\ 0 & d \end{bmatrix}, \tag{16}$$

where

$$b \neq 0 \quad \text{and} \quad (a, d) \neq (\pm 1, \mp 1) \tag{17}$$

excludes the reflections.

Moreover, because in the set of room–trajectory configurations with the same PPDMs any room from the set can be a

reference room, there is a symmetry between the reference $\mathcal{R}^0$ and the equivalent $\mathcal{R}$, so $\mathbf{T}^\top$ should be invertible. In other words, the determinant of $\mathbf{T}^\top$ must be non-zero, or, equivalently, $a \neq 0$ and $d \neq 0$.

3) *Reference room:* To find a reference room, we solve (14) for the normals $\{\varphi_k^0\}_{k=1}^K$. We observe that

$$\begin{aligned}&(a\cos\varphi_k^0 + b\sin\varphi_k^0)^2 + (d\sin\varphi_k^0)^2\\ &\quad = \cos\varphi_k^2 + \sin\varphi_k^2 = 1,\end{aligned} \tag{18}$$

so the angles of the reference room cannot be chosen arbitrarily. To find the values of $\{\varphi_k^0\}_{k=1}^K$ with respect to parameters a, b and d, we solve (18) and obtain

$$A\cos^2(2\varphi_k^0) + B\cos(2\varphi_k^0) + C = 0, \tag{19}$$

where

$$\begin{aligned}A &= (a^2 - b^2 - d^2)^2 + 4a^2b^2,\\ B &= 2(a^2 - b^2 - d^2)(a^2 + b^2 + d^2 - 2),\\ C &= (a^2 + b^2 + d^2 - 2)^2 - 4a^2b^2.\end{aligned} \tag{20}$$

Let first $A = 0$. Then (19) has two solutions: $a = 0, b^2 = -d^2$ and $b = 0$, $a^2 = d^2 = 1$. The first one makes (19) inconsistent, while the second one violates (17).

For $A \neq 0$, we have

$$\cos(2\varphi_k^0) = \frac{-B \pm \sqrt{B^2 - 4AC}}{2A}. \tag{21}$$

There are eight solutions for φ_k^0, four of which satisfy (14). The valid solutions always come as pairs $(\varphi_1^0, \varphi_2^0) = (\varphi_1^0, \varphi_1^0 + \pi)$ and $(\varphi_3^0, \varphi_4^0) = (\varphi_3^0, \varphi_3^0 + \pi)$.

4) *Equivalent rooms:* From (13), we identify the transformation that takes the normals of the reference room to the normals of an equivalent room. The corresponding angles in the equivalent room are computed from (14),

$$\begin{aligned}\varphi_k &= f(\varphi_k^0, s_k, a, b, d)\\ &= \operatorname{atan}\frac{d\sin\varphi_k^0}{a\cos\varphi_k^0 + b\sin\varphi_k^0} + s_k\pi,\end{aligned} \tag{22}$$

where $s_k \in \{0, 1\}$.

5) *Corresponding trajectories:* Next, we find the waypoints $\{\mathbf{r}_n^0\}_{n=1}^N$ and $\{\mathbf{r}_n\}_{n=1}^N$ that lie in the nullspace of $\bar{\mathbf{N}}^\top$. The nullspace is spanned by:

$$\begin{aligned}\mathbf{v}_1 &= \begin{bmatrix}-a, & -b, & 1, & 0\end{bmatrix}^\top,\\ \mathbf{v}_2 &= \begin{bmatrix}0, & -d, & 0, & 1\end{bmatrix}^\top,\end{aligned}$$

so the columns of $\bar{\mathbf{R}}$ are of the form

$$\begin{bmatrix}\mathbf{r}_n^0\\ -\mathbf{r}_n\end{bmatrix} = \mathbf{v}_1\gamma_1 + \mathbf{v}_2\gamma_2, \tag{23}$$

where $\gamma_1, \gamma_2 \in \mathbb{R}$. The waypoints in the reference room are chosen without restrictions, while the waypoints in the equivalent room are obtained by applying a non-rigid transformation

$$\mathbf{r}_n = (\mathbf{T}^\top)^{-1}\mathbf{r}_n^0. \tag{24}$$

This transformation corresponds to shearing followed by scaling. To show that, without loss of generality we can consider a reference room to be rectangular, so that $\varphi_1^0 = \pi/2$ and $\varphi_2^0 = \pi$. Then, (19) simplifies to $A - B + C = 0$ and $A + B + C = 0$ for $k = 1$ and $k = 2$, respectively, which further implies that $a^2 + d^2 = 1$ and $b^2 = 1$. The matrix $(\mathbf{T}^\top)^{-1}$ can be factorized into a product of a scaling matrix and a shear matrix as:

$$(\mathbf{T}^\top)^{-1} = \begin{bmatrix}\frac{1}{a} & 0\\ 0 & \frac{1}{d}\end{bmatrix}\begin{bmatrix}1 & 0\\ \pm\frac{1}{a} & 1\end{bmatrix},$$

with $a^2 + d^2 = 1$.

6) *Configurations with the same PPDMs:* The solutions of (21) suggest that we can construct a reference room by arbitrarily choosing two wall normals, φ_1^0 and φ_3^0, and solving the system of two equations (19) with $k \in \{1, 3\}$. This fixes two parameters (e.g., a and b) in $\mathbf{T}$ and leaves the third (e.g., d) free to generate an infinite number of rooms equivalent to the reference room. Reference rooms are not restricted to only two walls; we can have any number of additional walls parallel to those determined by φ_1^0 and φ_3^0, since they also satisfy (21).

A room–trajectory configuration $\mathcal{R}^0$ with walls $\{\mathcal{P}_k^0\}_{k=1}^K = \{(\mathbf{n}_k^0, q_k^0)\}_{k=1}^K$ and waypoints $\{\mathbf{r}_n^0\}_{n=1}^N$ is a generator of a set of room–trajectory configurations with identical PPDMs. The wall normals $\mathbf{n}_k^0$ are chosen as described above and the waypoints are arbitrary, $\mathbf{r}_n^0 \in \mathbb{R}^m$ for $1 \leq n \leq N$. The above analysis defines the following set of room–trajectory configurations with the same PPDMs:

$$\begin{aligned}\left[\mathcal{R}^0\right] = \big\{\mathcal{R}\,\big|\,&\varphi_k = f(\varphi_k^0, s_k, a, b, d),\\ &a \in \mathbb{R}\setminus\{0\}, b \in \mathbb{R}, d \in \mathbb{R}\setminus\{0\} \text{ s.t. } (17) \text{ holds, and,}\\ &a \in \mathbb{R}\setminus\{0\}, b \in \mathbb{R} \text{ s.t. } (19) \text{ holds for } k \in \{1, 3\},\\ &s_k \in \{0, 1\}, q_k = q_k^0 \text{ for } 1 \leq k \leq K,\\ &\mathbf{r}_n \text{ s.t. } (23) \text{ satisfied for } 1 \leq n \leq N\big\}.\end{aligned} \tag{25}$$

There are no constraints on the distances of walls from the origin in the reference room and we can set $\mathbf{q}^0$ arbitrarily. We note that this set of equivalent rooms with respect to PPDMs includes parallelogram rooms for $K = 4$, $\varphi_2^0 = \varphi_1^0 + \pi$ and $\varphi_4^0 = \varphi_3^0 + \pi$.

An example of three parallelogram configurations with the same PPDM is illustrated in Fig. 3.

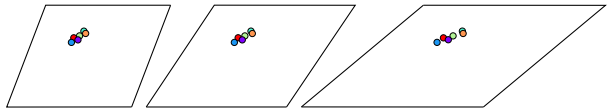

Fig. 3. Parallelogram rooms with the same PPDM.

B. 2D Rank-1: Infinitely Long Corridors

1) *Linear dependence:* In 2D, setting $\operatorname{rank}(\bar{\mathbf{N}}) = 1$ leads to degenerate rooms. To show that, assume that every column of $\bar{\mathbf{N}}^\top$ is a scaled version of the first column,

$$\begin{bmatrix}\sin\varphi_k^0\\ \cos\varphi_k\\ \sin\varphi_k\end{bmatrix} = \mathbf{T}\cos\varphi_k^0, \text{ where } \mathbf{T} = \begin{bmatrix}a\\ b\\ c\end{bmatrix}. \tag{26}$$

2) *Reparametrization:* These dependencies can be partially expressed as a transformation of the normals of the reference

room to those of the equivalent room. From (26) we have:

$$\begin{bmatrix}\cos\varphi_k\\ \sin\varphi_k\end{bmatrix} = \mathbf{T}'\begin{bmatrix}\cos\varphi_k^0\\ \sin\varphi_k^0\end{bmatrix},\ \text{where } \mathbf{T}' = \begin{bmatrix}b & 0\\ c & 0\end{bmatrix}. \tag{27}$$

With $c = 0$, $\mathbf{T}'$ becomes upper triangular. This eliminates rotations and reflections. Propagating back to $\mathbf{T}$, we get:

$$\mathbf{T} = \begin{bmatrix}a,\ b,\ 0\end{bmatrix}^\top. \tag{28}$$

3) *Reference room:* We see that (26) constrains the normals of the reference room, since

$$\tan\varphi_k^0 = a \tag{29}$$

must hold for every k. That is, the wall normals of the reference room cannot be chosen arbitrarily. Letting $s_k \in \{0, 1\}$, we summarize both solutions to (29) as

$$\varphi_k^0 = f(s_k, a) = \operatorname{atan} a + s_k\pi. \tag{30}$$

This implies that every φ_k^0 can only assume two values. For $K \geq 2$ walls, these values correspond to parallel walls since $\varphi_i^0 = \varphi_k^0 + \pi$ for $s_i = 0$ and $s_k = 1$.

4) *Equivalent rooms:* From (26) and (28) we have $\varphi_k \in \{0, \pi\}$ and

$$a^2 + 1 = b^2. \tag{31}$$

5) *Corresponding trajectories:* Though all rooms in this set have the same geometry, there are infinitely many trajectories that lead to the same PPDM. To see this, imagine an infinite corridor with two parallel walls. The points on any line parallel to the walls cannot be discriminated from distances to walls. Formally, a basis for the nullspace of $\bar{\mathbf{N}}^\top$ is

$$\mathbf{v}_1 = \begin{bmatrix}-a\\ 1\\ 0\\ 0\end{bmatrix}, \mathbf{v}_2 = \begin{bmatrix}-b\\ 0\\ 1\\ 0\end{bmatrix}, \mathbf{v}_3 = \begin{bmatrix}0\\ 0\\ 0\\ 1\end{bmatrix},$$

so the columns of $\bar{\mathbf{R}}$ have to be of the form

$$\begin{bmatrix}\mathbf{r}_n^0\\ -\mathbf{r}_n\end{bmatrix} = \gamma_1\mathbf{v}_1 + \gamma_2\mathbf{v}_2 + \gamma_3\mathbf{v}_3, \tag{32}$$

where γ_1, γ_2 and $\gamma_3 \in \mathbb{R}$. This further implies that the waypoints of the reference room $\{\mathbf{r}_n^0\}_{n=1}^N$ and the y coordinates of $\{\mathbf{r}_n\}_{n=1}^N$ in the equivalent rooms are independent and they can be chosen arbitrarily. The x coordinates of $\{\mathbf{r}_n\}_{n=1}^N$ are given by (32).

6) *Configurations with the same PPDMs:* This trivial case results in the set of room–trajectory configurations, in which the rooms have parallel walls. They are generated by a reference room $\{\mathcal{P}_k^0\}_{k=1}^K$ with the wall normals from (30), $\mathbf{q}^0 \in \mathbb{R}^K$, and arbitrary waypoints $\mathbf{r}_n^0 \in \mathbb{R}^m$ for $1 \leq n \leq N$,

$$\begin{aligned}&\left[\mathcal{R}^0\right] = \left\{\mathcal{R}\,\middle|\,\varphi_k \in \{0, \pi\}\right.,\\ &a \in \mathbb{R}, b \in \mathbb{R} \text{ s.t. } (31) \text{ satisfied},\\ &s_k \in \{0, 1\},\ q_k = q_k^0,\ \text{for } 1 \leq k \leq K,\\ &\left.\mathbf{r}_n \text{ s.t. } (32) \text{ satisfied for } 1 \leq n \leq N\right\}.\end{aligned} \tag{33}$$

Fig. 4 shows three equivalent configurations that emerge from this case.

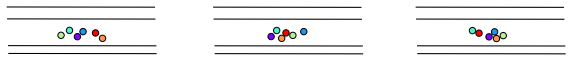

Fig. 4. Example of three equivalent infinitely long corridors.

C. 2D Rank-3: Linear Trajectories

1) *Linear dependence:* We assume $\operatorname{rank}(\bar{\mathbf{N}}) = 3$ so that

$$\cos\varphi_k = \mathbf{T}\begin{bmatrix}\sin\varphi_k\\ \cos\varphi_k^0\\ \sin\varphi_k^0\end{bmatrix},\ \text{where } \mathbf{T} = \begin{bmatrix}a & b & c\end{bmatrix}. \tag{34}$$

2) *Reparametrization:* As $r > m$, we cannot rewrite (34) such that the wall normals of $\mathcal{R}$ and $\mathcal{R}^0$ are on the opposite sides of the equation, so we omit this step.

3) *Reference room:* From (34), we observe that the wall orientations of the reference room are unconstrained.

4) *Equivalent rooms:* We can express the wall orientations φ_k in the equivalent room as a function of φ_k^0 and entries in $\mathbf{T}$,

$$\begin{aligned}\varphi_k &= f(\varphi_k^0, s_k, a, b, c)\\ &= s_k\operatorname{acos}\frac{b\cos\varphi_k^0 + c\sin\varphi_k^0}{\sqrt{a^2+1}} - \operatorname{atan} a,\end{aligned} \tag{35}$$

where $s_k \in \{-1, 1\}$ and the parameters a, b and c are such that

$$\begin{aligned}&|\, b\cos\varphi_k^0 + c\sin\varphi_k^0 \,| \leq \sqrt{a^2+1} \quad \text{for every } \varphi_k^0,\\ &1 \leq k \leq K.\end{aligned} \tag{36}$$

5) *Corresponding trajectories:* The nullspace of $\bar{\mathbf{N}}^\top$ is spanned by one vector $\mathbf{v}_1 = \begin{bmatrix}-b & -c & 1 & -a\end{bmatrix}^\top$, so the columns of $\bar{\mathbf{R}}$ satisfy

$$\begin{bmatrix}\mathbf{r}_n^0\\ -\mathbf{r}_n\end{bmatrix} = \mathbf{v}_1\gamma, \tag{37}$$

where $\gamma \in \mathbb{R}$. This can be further rewritten as

$$\mathbf{r}_n = \mathbf{S}\mathbf{r}_n^0 \quad \text{and} \tag{38}$$

$$r_{n,y}^0 = \frac{c}{b}r_{n,x}^0, \tag{39}$$

where $\mathbf{S}$ is a scaling matrix with $\frac{1}{b}$ and $-\frac{a}{c}$ on a diagonal, $b \neq 0$, $c \neq 0$, and $\mathbf{r}_n^0 = [r_{n,x}^0, r_{n,y}^0]^\top$. This suggests that the x and y coordinates of the waypoints in both rooms are dependent, and the trajectories are linear. Furthermore, having $b \neq 0$ and $c \neq 0$ ensures that the waypoints in the reference room are not restricted to lie on the x-axis or the y-axis; the trajectories can be chosen arbitrarily as long as they are linear.

6) *Configurations with the same PPDMs:* A room–trajectory configuration $\mathcal{R}^0$, with an arbitrary room $\{\mathcal{P}_k^0\}_{k=1}^K$ and a linear trajectory $\{\mathbf{r}_n^0\}_{n=1}^N$ satisfying (39), generates the following set:

$$\begin{aligned}&\left[\mathcal{R}^0\right] = \left\{\mathcal{R}\,\middle|\,\varphi_k = f(\varphi_k^0, s_k, a, b, c),\right.\\ &a \in \mathbb{R}, b \in \mathbb{R}\setminus\{0\}, c \in \mathbb{R}\setminus\{0\} \text{ s.t. } (36) \text{ satisfied},\\ &s_k \in \{-1, 1\}, q_k = q_k^0,\ \text{for } 1 \leq k \leq K,\\ &\left.\mathbf{r}_n \text{ s.t. } (37) \text{ satisfied for } 1 \leq n \leq N\right\}.\end{aligned} \tag{40}$$

For any arbitrary room with K walls and a PPDM measured at collinear waypoints, we can find another room with the same PPDM obtained at different collinear waypoints; an example is shown in Fig. 5.

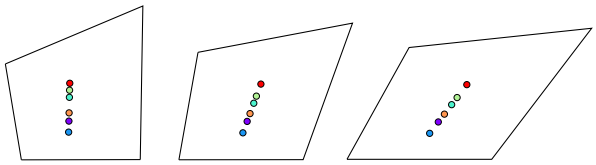

Fig. 5. Example of equivalent rooms with linear trajectories.

V. Classification of 3D Configurations

In 3D ($m = 3$) we analyze the cases $r \in \{1, 2, 3, 4, 5\}$.

A. 3D Rank-1: Infinitely Long and Tall Corridors

1) *Linear dependence:* When $\operatorname{rank}(\bar{\mathbf{N}}) = 1$ in 3D, five columns of $\bar{\mathbf{N}}^\top$ are scaled version of a single non-zero column,

$$\begin{bmatrix} \sin\theta_k^0 \sin\varphi_k^0 \\ \cos\theta_k^0 \\ \sin\theta_k \cos\varphi_k \\ \sin\theta_k \sin\varphi_k \\ \cos\theta_k \end{bmatrix} = \mathbf{T} \sin\theta_k^0 \cos\varphi_k^0, \text{ where } \mathbf{T} = \begin{bmatrix} a \\ b \\ c \\ d \\ e \end{bmatrix}. \quad (41)$$

2) *Reparametrization:* The requirement (41) implies the following relationship between the wall normals of the reference room and those of the equivalent room:

$$\begin{bmatrix} \sin\theta_k \cos\varphi_k \\ \sin\theta_k \sin\varphi_k \\ \cos\theta_k \end{bmatrix} = \begin{bmatrix} c & 0 & 0 \\ d & 0 & 0 \\ e & 0 & 0 \end{bmatrix} \begin{bmatrix} \sin\theta_k^0 \cos\varphi_k^0 \\ \sin\theta_k^0 \sin\varphi_k^0 \\ \cos\theta_k^0 \end{bmatrix}, \quad (42)$$

As before, we set $d = e = 0$ to get an upper triangular matrix, and $c \neq 0$ for a system to be consistent.

3) *Reference room:* From (41), it follows that

$$\tan\varphi_k^0 = a \quad \text{and} \quad \tan\theta_k^0 = \frac{1}{b\cos\varphi_k^0} \quad (43)$$

for every k. Then,

$$\varphi_k^0 = \operatorname{atan} a + s_k\pi, \quad (44)$$

$$\theta_k^0 = \begin{cases} \operatorname{atan}\frac{\sqrt{a^2+1}}{b} + t_k\pi & s_k = 0, \\ -\operatorname{atan}\frac{\sqrt{a^2+1}}{b} + t_k\pi & s_k = 1, \end{cases} \quad (45)$$

where $s_k, t_k \in \{0, 1\}$ are independent binary variables. That is, the reference room cannot be chosen arbitrarily; the angles can only assume two values that yield parallel walls.

4) *Equivalent rooms:* From (41) we also find that $\sin\varphi_k = 0$ and $\cos\theta_k = 0$, so the angle θ_k takes a value of $\pi/2$, while φ_k is either 0 or π, depending on the value of t_k. This dependence arises from the fact that

$$c = \begin{cases} b\cos\varphi_k\sqrt{\frac{a^2+b^2+1}{b^2}} & t_k = 0, \\ -b\cos\varphi_k\sqrt{\frac{a^2+b^2+1}{b^2}} & t_k = 1, \end{cases} \quad (46)$$

needs to be satisfied for every k for (41) to be consistent. Note that $b \neq 0$ is implied by $c \neq 0$.

5) *Corresponding trajectories:* Analogously to the rank-1 case in 2D, the ambiguity in the reconstruction is due to the multitude of consistent trajectories. Points in planes parallel to the walls cannot be uniquely determined from distances to the walls. The nullspace of $\bar{\mathbf{N}}^\top$ is spanned by five vectors,

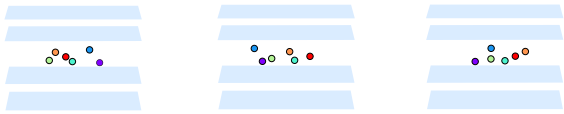

Fig. 6. Three equivalent infinitely long and tall corridors.

$$\mathbf{v}_1 = \begin{bmatrix} -a \\ 1 \\ 0 \\ 0 \\ 0 \\ 0 \end{bmatrix}, \mathbf{v}_2 = \begin{bmatrix} -b \\ 0 \\ 1 \\ 0 \\ 0 \\ 0 \end{bmatrix}, \mathbf{v}_3 = \begin{bmatrix} -c \\ 0 \\ 0 \\ 1 \\ 0 \\ 0 \end{bmatrix},$$

$$\mathbf{v}_4 = \begin{bmatrix} 0 \\ 0 \\ 0 \\ 0 \\ 1 \\ 0 \end{bmatrix}, \mathbf{v}_5 = \begin{bmatrix} 0 \\ 0 \\ 0 \\ 0 \\ 0 \\ 1 \end{bmatrix},$$

so the columns of $\bar{\mathbf{R}}$ are

$$\begin{bmatrix} \mathbf{r}_n^0 \\ -\mathbf{r}_n \end{bmatrix} = \gamma_1\mathbf{v}_1 + \gamma_2\mathbf{v}_2 + \gamma_3\mathbf{v}_3 + \gamma_4\mathbf{v}_4 + \gamma_5\mathbf{v}_5, \quad (47)$$

where $\gamma_1, \gamma_2, \gamma_3, \gamma_4$ and $\gamma_5 \in \mathbb{R}$. This implies that the waypoints $\{\mathbf{r}_n^0\}_{n=1}^N$ in the reference room and the y and z coordinates of $\{\mathbf{r}_n\}_{n=1}^N$ in the equivalent rooms are independent and can be chosen arbitrarily, whereas the x coordinates of $\{\mathbf{r}_n\}_{n=1}^N$ are given by (47).

6) *Configurations with the same PPDMs:* A set of these degenerate room–trajectory configurations with parallel walls is generated by a reference room $\{\mathcal{P}_k^0\}_{k=1}^K$ with the wall normals from (44), $\mathbf{q}^0 \in \mathbb{R}^K$, and arbitrary waypoints $\{\mathbf{r}_n^0\}_{n=1}^N$,

$$\begin{aligned} [\mathcal{R}^0] = \{\mathcal{R} \,|\, & \varphi_k \in \{0, \pi\}, \theta_k = \pi/2, \\ & a \in \mathbb{R}, b \in \mathbb{R}\backslash\{0\}, c \in \mathbb{R}\backslash\{0\} \text{ s.t. } (46) \text{ satisfied}, \\ & s_k \in \{0, 1\}, t_k \in \{0, 1\}, \\ & q_k = q_k^0, \text{ for } 1 \leq k \leq K, \\ & \mathbf{r}_n \text{ s.t. } (47) \text{ satisfied for } 1 \leq n \leq N\}. \end{aligned} \quad (48)$$

An example of such room–trajectory configurations is shown in Fig. 6.

B. 3D Rank-2: Parallelepipeds Without Bases

1) *Linear dependence:* Assume that the first and the second column are linearly independent, and the others are their linear combinations. Thus, for every wall k we have

$$\begin{bmatrix} \cos\theta_k^0 \\ \sin\theta_k \cos\varphi_k \\ \sin\theta_k \sin\varphi_k \\ \cos\theta_k \end{bmatrix} = \mathbf{T} \begin{bmatrix} \sin\theta_k^0 \cos\varphi_k^0 \\ \sin\theta_k^0 \sin\varphi_k^0 \end{bmatrix},$$

$$\text{where } \mathbf{T} = \begin{bmatrix} a & b \\ c & d \\ e & f \\ g & h \end{bmatrix}. \quad (49)$$

2) *Reparametrization:* As before, (49) implies a relationship between the normals of the reference and the equivalent room,

$$\begin{bmatrix}\sin\theta_k\cos\varphi_k\\ \sin\theta_k\sin\varphi_k\\ \cos\theta_k\end{bmatrix}=\begin{bmatrix}c & d & 0\\ e & f & 0\\ g & h & 0\end{bmatrix}\begin{bmatrix}\sin\theta_k^0\cos\varphi_k^0\\ \sin\theta_k^0\sin\varphi_k^0\\ \cos\theta_k^0\end{bmatrix}. \tag{50}$$

By setting e, g and h to 0, we obtain the desired upper triangular matrix and propagate this change into $\mathbf{T}$,

$$\mathbf{T}=\begin{bmatrix}a & c & 0 & 0\\ b & d & f & 0\end{bmatrix}^\top. \tag{51}$$

We also require that $c\neq 0$ and $f\neq 0$. Otherwise, all rooms in the set of room–trajectory configurations with the same PPDMs have identical geometries and the orientation of every wall of every room in the set is the same; this case has already been covered by rank-1 in 3D.

3) *Reference room:* The sum of the squares of the last three equations in (49) has to be 1 for every wall k,

$$\begin{aligned}&(c\sin\theta_k^0\cos\varphi_k^0+d\sin\theta_k^0\sin\varphi_k^0)^2\\ &\quad+(f\sin\theta_k^0\sin\varphi_k^0)^2=1,\end{aligned} \tag{52}$$

so the reference room cannot be chosen arbitrarily. From (52), we can express θ_k^0 as a function of φ_k^0 and the entries of $\mathbf{T}$.

The first equation in (49) additionally constrains θ_k^0 and φ_k^0,

$$\tan\theta_k^0=(a\cos\varphi_k^0+b\sin\varphi_k^0)^{-1}. \tag{53}$$

We obtain a quadratic equation with respect to $\cos(2\varphi_k^0)$,

$$\begin{aligned}&(A^2+B^2)\cos^2(2\varphi_k^0)-2\,AC\cos(2\varphi_k^0)\\ &\quad+(C^2-B^2)=0,\end{aligned} \tag{54}$$

where

$$\begin{aligned}A&=-a^2+b^2+c^2-d^2-f^2,\\ B&=2(ab-cd),\\ C&=a^2+b^2-c^2-d^2-f^2+2.\end{aligned} \tag{55}$$

We first assume $A^2+B^2\neq 0$ and solve (54) for φ_k^0,

$$\cos(2\varphi_k^0)=\frac{AC\pm\sqrt{A^2\,C^2-(A^2+B^2)(C^2-B^2)}}{A^2+B^2}. \tag{56}$$

We obtain four solutions for φ_k^0 to (54) that satisfy (49). For each value of φ_k^0 we can find the corresponding θ_k^0 from (52) or (53). Valid solutions always generate two pairs of wall normals: $\{\theta_k^0,\varphi_k^0\}_{k=1}^2=\{(\theta_1^0,\varphi_1^0),(-\theta_1^0,\varphi_1^0+\pi)\}$ and $\{\theta_k^0,\varphi_k^0\}_{k=3}^4=\{(\theta_3^0,\varphi_3^0),(-\theta_3^0,\varphi_3^0+\pi)\}$. Therefore, each reference room is made of two arbitrarily chosen walls and two walls parallel to them, resulting in parallelepipeds without its two bases.

As the case of $A^2+B^2=0$ results in rather different geometries, it is analyzed separately in Section V-C.

4) *Equivalent rooms:* The corresponding angles in the equivalent room are computed from (49),

$$\theta_k=\pi/2,\quad \varphi_k=g(\theta_k^0,\varphi_k^0,c,d,f)+s_k\pi, \tag{57}$$

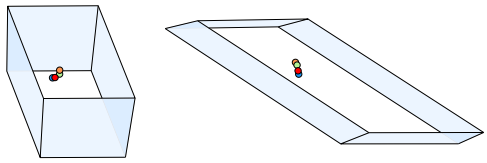

Fig. 7. Two parallelepipeds without bases with the same PPDM.

where $s_k\in\{0,1\}$ and

$$g(\theta_k^0,\varphi_k^0,c,d,f)=\operatorname{atan}\frac{f\sin\theta_k^0\sin\varphi_k^0}{c\sin\theta_k^0\cos\varphi_k^0+d\sin\theta_k^0\sin\varphi_k^0}. \tag{58}$$

5) *Corresponding trajectories:* The nullspace of $\bar{\mathbf{N}}^\top$ is spanned by four vectors,

$$\mathbf{v}_1=\begin{bmatrix}-a\\-b\\1\\0\\0\\0\end{bmatrix},\mathbf{v}_2=\begin{bmatrix}-c\\-d\\0\\1\\0\\0\end{bmatrix},\mathbf{v}_3=\begin{bmatrix}0\\-f\\0\\0\\1\\0\end{bmatrix},\mathbf{v}_4=\begin{bmatrix}0\\0\\0\\0\\0\\1\end{bmatrix},$$

so the waypoints in $\bar{\mathbf{R}}$ are related as

$$\begin{bmatrix}\mathbf{r}_n^0\\-\mathbf{r}_n\end{bmatrix}=\gamma_1\mathbf{v}_1+\gamma_2\mathbf{v}_2+\gamma_3\mathbf{v}_3+\gamma_4\mathbf{v}_4, \tag{59}$$

where $\gamma_1,\gamma_2,\gamma_3$ and $\gamma_4\in\mathbb{R}$. It follows that the waypoints of the reference room are independent and can be chosen arbitrarily, whereas the corresponding waypoints of the equivalent rooms are given by (59).

6) *Configurations with the same PPDMs:* We can set two wall orientations of a reference room by arbitrarily choosing φ_1^0 and φ_3^0, and by computing θ_1^0 and θ_3^0 from (53). By solving the system of two equations (54) with $k\in\{1,3\}$, we fix two parameters (e.g., c and d) and leave the third parameter (e.g., f) free to generate new rooms equivalent to the reference. Walls parallel to those defined by (θ_1^0,φ_1^0) and (θ_3^0,φ_3^0) are determined by $(-\theta_1^0,\varphi_1^0+\pi)$ and $(-\theta_3^0,\varphi_3^0+\pi)$. Recall that the solutions of (54) always come in pairs $(\theta_k^0,-\theta_k^0)$ and $(\varphi_k^0,\varphi_k^0+\pi)$, so adding walls parallel to the two fixed ones does not violate (54).

As usual, we can choose $\mathbf{q}^0\in\mathbb{R}^K$ arbitrarily, and define a set of room–trajectory configurations with the same PPDM as $\mathcal{R}^0$, where $\{\mathcal{P}_k^0\}_{k=1}^K$ is described above and $\{\mathbf{r}_n^0\}_{n=1}^N$ is arbitrary:

$$\begin{aligned}\left[\mathcal{R}^0\right]=\big\{\mathcal{R}\,\big|\,&\varphi_k=g(\theta_k^0,\varphi_k^0,c,d,f)+s_k\pi,\theta_k=\pi/2,\\ &c\in\mathbb{R}\setminus\{0\},d\in\mathbb{R}\text{ s.t. }(54)\text{ satisfied},f\in\mathbb{R}\setminus\{0\},\\ &s_k\in\{0,1\},q_k=q_k^0,\text{ for }1\le k\le K,\\ &\mathbf{r}_n\text{ s.t. }(59)\text{ satisfied for }1\le n\le N\big\}.\end{aligned} \tag{60}$$

An example is illustrated in Fig. 7.

C. 3D Rank-2: Prisms Without Bases

In step 3 of the previous case, we studied $A^2+B^2\neq 0$. Now we focus on $A^2+B^2=0$ and omit steps 1 and 2 as they are identical to Section V-B.

3) *Reference room:* The case of $A^2+B^2=0$ leads to $A=B=C=0$ and (54) being satisfied for any value of φ_k^0. By

solving $A = B = C = 0$, we find explicit expressions for three dependent parameters in $\mathbf{T}$,

$$c = \pm\sqrt{a^2+1},\ d = \pm\frac{ab}{\sqrt{a^2+1}},$$
$$f = \pm\sqrt{b^2 - \frac{a^2b^2}{a^2+1} + 1}. \tag{61}$$

Then, from arbitrarily chosen angles φ_k^0, and the parameters in $\mathbf{T}$ that satisfy (61), we compute θ_k^0 from (52) or (53). Such a room consists of K walls parallel to a fixed line; this means that every triplet of walls forms a prismatic surface, or equivalently, every wall intersects the other two along lines.

To see this, observe that the rank of the coefficient matrix $\mathbf{N}^0$ is 2, while the rank of the augmented matrix $\mathbf{M}^0$,

$$\mathbf{M}^{0\top} = \begin{bmatrix}\mathbf{N}^{0\top} & \mathbf{q}\end{bmatrix}, \tag{62}$$

can be 2 or 3. Indeed, the coefficient matrix from (53) is

$$\mathbf{n}_k^0 = \frac{1}{\sqrt{1+(a\cos\theta_k^0 + b\sin\theta_k^0)^2}}\begin{bmatrix}\cos\varphi_k^0\\ \sin\varphi_k^0\\ a\cos\varphi_k^0 + b\sin\varphi_k^0\end{bmatrix}. \tag{63}$$

The third row of $\mathbf{N}^{0\top}$ is a linear combination of the first two rows so $\mathrm{rank}(\mathbf{N}^0) = 2$. From (62) it follows that $\mathrm{rank}(\mathbf{M}^0) = 3$, except for a set of $\mathbf{q}$ of Lebesgue measure zero. A specific case of $\mathrm{rank}(\mathbf{M}^0) = 2$ occurs when the values of $\mathbf{q}$ are chosen so that all walls intersect in one line.

4) *Equivalent rooms:* The angles of the equivalent room θ_k and φ_k are computed from (57). We show that the equivalent room is a rotated version of the reference room.

The rotation ambiguity exists despite the reparametrization in step 2 because the normals in any equivalent room lie in a plane (the xy-plane in the reference room). Then, transformation of the normals of $\{\mathcal{P}_k^0\}_{k=1}^K$ to those of $\{\mathcal{P}_k\}_{k=1}^K$ is determined by two angles, instead of three for a general rotation. We can factor any upper triangular matrix into a product of a rotation matrix around two axes and a square matrix by two Givens rotations [43]. Thus, $\mathbf{T}$ being upper-triangular still allows for rotations specified by two angles.

We introduce a matrix $\mathbf{R} = (r_{ij})_{i,j=1}^3$ such that

$$\begin{bmatrix}\sin\theta_k\cos\varphi_k\\ \sin\theta_k\sin\varphi_k\\ \cos\theta_k\end{bmatrix} = \mathbf{R}\begin{bmatrix}\sin\theta_k^0\cos\varphi_k^0\\ \sin\theta_k^0\sin\varphi_k^0\\ \cos\theta_k^0\end{bmatrix} \text{ for } 1\le k\le K. \tag{64}$$

Together with (50), we obtain

$$c = r_{11} + ar_{13},\quad d = r_{12} + br_{13},\quad 0 = r_{21} + ar_{23},$$
$$f = r_{22} + br_{23},\quad 0 = r_{31} + ar_{33},\quad 0 = r_{32} + br_{33}, \tag{65}$$

so we can rewrite $\mathbf{R}$ as

$$\mathbf{R} = \begin{bmatrix}c - ar_{13} & d - br_{13} & r_{13}\\ -ar_{23} & f - br_{23} & r_{23}\\ -ar_{33} & -br_{33} & r_{33}\end{bmatrix} =$$
$$= \begin{bmatrix}c & d & 0\\ 0 & f & 0\\ 0 & 0 & 0\end{bmatrix} - \begin{bmatrix}r_{13}\\ r_{23}\\ r_{33}\end{bmatrix}\begin{bmatrix}a & b & -1\end{bmatrix}. \tag{66}$$

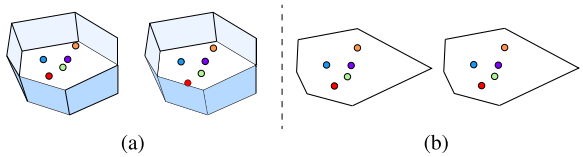

Fig. 8. Two prisms without bases with the same PPDM. (a) The rooms are identical, but the waypoints differ. (b) A bird's eye view. The configurations from this angle seem identical.

To see that $\mathbf{R}$ is a rotation, note that from $A = B = C = 0$, (66), and (55), the columns of $\mathbf{R}$ are orthonormal.

5) *Corresponding trajectories:* The dependence of the corresponding waypoints is given in (59) with an additional constraint on the parameters in (61). Intuitively, any waypoint that lies on a line parallel to walls generates the same PPDM.

6) *Configurations with the same PPDMs:* It follows that two equivalent rooms in the rank-2 case in 3D with $A^2 + B^2 = 0$ have identical geometries, but could have different waypoints lying on a line parallel to all walls; see Fig. 8.

D. 3D Rank-3: Miscellaneous Geometries

1) *Linear dependence:* The practically relevant shoebox rooms generate configurations not uniquely determined by PPDMs. For $\mathrm{rank}(\bar{\mathbf{N}}) = 3$,

$$\begin{bmatrix}\sin\theta_k\cos\varphi_k\\ \sin\theta_k\sin\varphi_k\\ \cos\theta_k\end{bmatrix} = \mathbf{T}\begin{bmatrix}\sin\theta_k^0\cos\varphi_k^0\\ \sin\theta_k^0\sin\varphi_k^0\\ \cos\theta_k^0\end{bmatrix}, \tag{67}$$

where

$$\mathbf{T} = \begin{bmatrix}a & b & c\\ d & e & f\\ g & h & i\end{bmatrix}. \tag{68}$$

2) *Reparametrization:* We make $\mathbf{T}$ upper triangular matrix by setting d, g and h to 0. Similarly as for the case of rank-2 in 2D, we also ensure that $\mathbf{T}$ be invertible by requiring $a \neq 0$, $e \neq 0$ and $i \neq 0$. Moreover, to exclude reflections we assume that

$$(a,e,i) \neq (-1,1,1),$$
$$(a,e,i) \neq (1,-1,1),$$
$$(a,e,i) \neq (1,1,-1). \tag{69}$$

3) *Reference room:* Since in (67) we have three equations with four angles for every wall k, we can express θ_k^0, θ_k and φ_k in terms of an arbitrarily chosen angle φ_k^0 and the parameters in $\mathbf{T}$. Squaring and summing (67) gives

$$0 = (A^2+B^2)\sin^2(2\theta_k^0) + 2(A+2C)B\sin(2\theta_k^0) + 4\,C(A+C), \tag{70}$$

where

$$A = a^2\cos^2\varphi_k^0 + (b^2+e^2)\sin^2\varphi_k^0 + 2ab\sin\varphi_k^0\cos\varphi_k^0 - C - 1,$$
$$B = ac\cos\varphi_k^0 + (bc+ef)\sin\varphi_k^0,$$
$$C = c^2 + f^2 + i^2 - 1. \tag{71}$$

To find θ_k^0, we solve (70) and obtain

$$\cos(2\theta_k^0) = x_1 \quad \text{or} \quad \cos(2\theta_k^0) = x_2, \tag{72}$$

with

$$x_{1,2} = \frac{A(A+2\,C) \pm B\sqrt{B^2 - 4AC - 4\,C^2}}{A^2 + B^2}. \tag{73}$$

We first consider $A^2 + B^2 \neq 0$, while the case of $A^2 + B^2 = 0$ is analyzed separately in Section V-E. Analogously to the rank-2 case in 2D or 3D, not all solutions to (72) satisfy (67); the four valid values of θ_k^0 are identified by verifying

$$\begin{aligned} 1 = {} & (a \sin\theta_k^0 \cos\varphi_k^0 + b \sin\theta_k^0 \sin\varphi_k^0 + c\cos\theta_k^0)^2 \\ & + (e \sin\theta_k^0 \sin\varphi_k^0 + f\cos\theta_k^0)^2 + i^2\cos^2\theta_k^0 \end{aligned} \tag{74}$$

for $1 \leq k \leq K$. Contrary to the rank-2 case in 2D or 3D, the values of A, B and C in (72) depend on φ_k^0 and the solutions to (72) vary for different walls k. We denote them $\theta_{k,1}^0$, $\theta_{k,2}^0$, $\theta_{k,3}^0$ and $\theta_{k,4}^0$, where $\theta_{k,1}^0$ and $\theta_{k,2}^0$ are computed from x_1, while $\theta_{k,3}^0$ and $\theta_{k,4}^0$ from x_2. They satisfy $\theta_{k,2}^0 = \theta_{k,1}^0 + \pi$ and $\theta_{k,4}^0 = \theta_{k,3}^0 + \pi$.

For some fixed parameters in $\mathbf{T}$, there are infinitely many ways to arrange the walls of the reference room. The angles $\{\varphi_k^0\}_{k=1}^K$ are chosen from $[0, 2\pi)$, while $\{\theta_k^0\}_{k=1}^K$ are computed from (72) and (73). For any arbitrarily chosen φ_k^0, there are four values of θ_k^0 that satisfy (74), $\theta_{k,1}^0 \ldots, \theta_{k,4}^0$. This allows us to create up to four different walls for one fixed value of φ_k^0. For example, in one case, for a chosen φ_k^0 we can choose only one value θ_{k,j_k}^0, $1 \leq j_k \leq 4$, and create wall normals $\{\theta_{k,j_k}^0, \varphi_k^0\}_{k=1}^K$. Such rooms have different angles for every wall. In another case, some rooms can have one value φ_k^0 associated to four walls, $\{\theta_{k,1}^0, \varphi_k^0\}_{k=1}^{K/4}$, $\{\theta_{k,2}^0, \varphi_k^0\}_{k=1}^{K/4}$, $\{\theta_{k,3}^0, \varphi_k^0\}_{k=1}^{K/4}$ and $\{\theta_{k,4}^0, \varphi_k^0\}_{k=1}^{K/4}$.

We denote the number of independent walls (i.e., different values of φ_k^0) by K_0. We can create reference rooms for any K_0 and given $\mathbf{T}$ by the procedure described above. However, as the parameters in $\mathbf{T}$ need to be fixed to compute θ_k^0 from φ_k^0, for every reference room there is only one equivalent room, computed from (67).

A result that is in line with our previous analysis occurs for $K_0 < 6$. Then, we can construct a reference room with *any* K_0 walls $\{\theta_k^0, \varphi_k^0\}_{k=1}^{K_0}$. Furthermore, we can add walls parallel to these K_0 walls without additionally constraining (74), so we can have up to $K = 2K_0 < 12$ walls in the reference room. Then, we can solve the system of K_0 equations (74) with $1 \leq k \leq K_0$ to find K_0 dependent parameters in $\mathbf{T}$, and generate new equivalent rooms from (67) by changing the remaining $6 - K_0$ free parameters in $\mathbf{T}$.

4) *Equivalent rooms:* The transformation to equivalent rooms is the same for all reference rooms and we find it from (67),

$$\theta_k = t_k f(\theta_k^0, i), \qquad \varphi_k = g(\theta_k^0, \varphi_k^0, \mathbf{T}) + s_k\pi, \tag{75}$$

where

$$\begin{aligned} f(\theta_k^0, i) &= \operatorname{acos}\,(i\cos\theta_k^0), \\ g(\theta_k^0, \varphi_k^0, \mathbf{T}) &= \operatorname{atan} \\ &\quad \times \frac{e\sin\theta_k^0 \sin\varphi_k^0 + f\cos\theta_k^0}{\sin\theta_k^0(a\cos\varphi_k^0 + b\sin\varphi_k^0) + c\cos\theta_k^0}, \end{aligned} \tag{76}$$

Fig. 9. A pair of equivalent rooms in 3D.

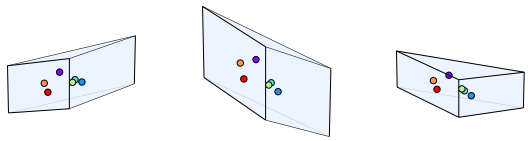

Fig. 10. Rooms with less than six walls in 3D with identical PPDMs.

$t_k \in \{-1, 1\}$ and $s_k \in \{0, 1\}$. The choice of t_k uniquely determines s_k, such that (67) is satisfied.

5) *Corresponding trajectories:* The nullspace of $\bar{\mathbf{N}}^\top$ is spanned by three vectors in all of the aforementioned cases,

$$\begin{aligned} \mathbf{v}_1 &= \left[-a,\ -b,\ -c,\ 1,\ 0,\ 0\right]^\top, \\ \mathbf{v}_2 &= \left[0,\ -e,\ -f,\ 0,\ 1,\ 0\right]^\top, \\ \mathbf{v}_3 &= \left[0,\ 0,\ -i,\ 0,\ 0,\ 1\right]^\top. \end{aligned}$$

Then,

$$\begin{bmatrix} \mathbf{r}_n^0 \\ -\mathbf{r}_n \end{bmatrix} = \mathbf{v}_1\gamma_1 + \mathbf{v}_2\gamma_2 + \mathbf{v}_3\gamma_3, \tag{77}$$

where γ_1, γ_2 and $\gamma_3 \in \mathbb{R}$. The waypoints in one room are chosen arbitrarily and a non-rigid transformation $\mathbf{T}^\top$ is applied to compute the waypoints in the equivalent room, $\mathbf{r}_n = (\mathbf{T}^\top)^{-1}\mathbf{r}_n^0$.

6) *Configurations with the same PPDMs:* A set of room–trajectory configurations with the same PPDMs is given as

$$\begin{aligned} \left[\mathcal{R}^0\right] = \big\{ & \mathcal{R} \,\big|\, \varphi_k = g(\theta_k^0, \varphi_k^0, \mathbf{T}) + s_k\pi, \theta_k = t_k f(\theta_k^0, i), \\ & K_0 < 6 \text{ values from } \{a, b, c, e, f, i\} \in \mathbb{R} \text{ s.t. (74) satisfied}, \\ & \text{the remaining } 6 - K_0 \text{ values from } \{a, b, c, e, f, i\} \in \mathbb{R}, \\ & a, b, c, e, f, i \text{ s.t. (69) satisfied, and } a \neq 0, e \neq 0, i \neq 0, \\ & t_k \in \{-1, 1\}, s_k \in \{0, 1\} \text{ s.t. (67) satisfied}, \\ & q_k = q_k^0, \text{ for } 1 \leq k \leq K, \\ & \mathbf{r}_n \text{ s.t. (77) satisfied for } 1 \leq n \leq N\big\}, \end{aligned} \tag{78}$$

where the waypoints in the reference room are chosen arbitrarily, while the reference room $\{\mathcal{P}_k^0\}_{k=1}^K$ can have at most $K_0 < 6$ arbitrarily chosen walls and K_0 walls parallel to them.

Two room–trajectory configurations that correspond to $K_0 = K = 6$ are shown in Fig. 9. The angles $\{\varphi_k^0\}_{k=1}^K$ of the reference room (left) and the parameters in $\mathbf{T}$ are chosen arbitrarily, while $\theta_{k_j}^0$ for $j = 1, \ldots, 4$ are computed from (72) and (73). For every k, only one value of $\{\theta_{k_j}^0\}_{k=1}^K$ is assigned to the wall k. For such a reference room, there is only one equivalent room (right), with wall normals from (75).

An example of an arbitrarily chosen room with five walls ($K_0 = K = 5$) together with the two room–trajectory configurations with the same PPDMs (78) is shown in Fig. 10.

Fig. 11 illustrates an example of arbitrarily chosen three pairs of parallel walls in a room, $K_0 = 3$, together with the two rooms from the same set (78).

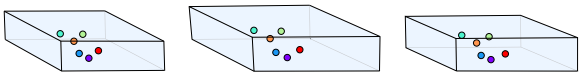

Fig. 11. An example of equivalent rooms with three pairs of parallel walls.

E. 3D Rank-3: Two Sets of Parallel Walls

There is another set of room–trajectory configurations with the same PPDMs arising from $\operatorname{rank}(\bar{\mathbf{N}}) = 3$ for $A^2 + B^2 = 0$ and $\cos\varphi_k^0 \neq 0$. One can show that these constraints lead to rooms with arbitrarily chosen angles θ_k^0 and constant values for φ_k^0 (up to a shift by π), i.e., rooms with all walls parallel to a line. An analysis similar to that in Section V-C shows that the rooms in the same set are simply rotated versions of the reference room.

1) *Reference room:* We continue with $A^2 + B^2 = 0$ which implies $A = B = C = 0$, and in addition we assume that $\cos\varphi_k^0 = 0$. We omit steps 1, 2 and 5 as they are identical to Section V-C. From $B = 0$, it follows that

$$ac = 0 \quad \text{and} \quad bc + ef = 0. \tag{79}$$

From (79), we conclude that either $a \neq 0, c = 0$, or $a = 0, c \neq 0$, or $a = c = 0$. The last two cases are not of our interest as $a = 0$ implies that the x coordinates of $\mathbf{r}_n^0$ are 0, and the points lie in the yz-plane. Such a degenerate trajectory is covered in our next case, $\operatorname{rank}(\bar{\mathbf{N}}) = 4$, so we do not study it further here. A similar observation can be made for $a \neq 0, c = 0, e = 0$; the y coordinates of $\mathbf{r}_n^0$ are proportional to their x coordinates, so the points lie in a plane, which corresponds to $\operatorname{rank}(\bar{\mathbf{N}}) = 4$.

A new set of room–trajectory configurations with the same PPDMs arises for $a \neq 0, c = 0, f = 0$. From $C = 0$, we obtain that $i = \pm 1$, while $A = 0$ defines φ_k^0,

$$(a\cos\varphi_k^0 + b\sin\varphi_k^0)^2 + e^2\sin^2\varphi_k^0 = 1. \tag{80}$$

By introducing $u = \tan\frac{\varphi_k^0}{2}$ and $z = \frac{u^2-1}{u}$, we can find the solutions of (80) in terms of z,

$$z_{1,2} = \frac{2ab \pm 2\sqrt{-a^2e^2 + a^2 + b^2 - e^2 - 1}}{a^2 - 1}, \tag{81}$$

from which we can express the four solutions of φ_k^0,

$$\varphi_k^0 = 2\operatorname{atan}\frac{z_j \pm \sqrt{z_j^2 + 4}}{2}, \tag{82}$$

for $j \in \{1, 2\}$. We observe that the normals computed from z_1 generate rooms with walls parallel to a certain line ℓ_1. Analogously, the normals generated by z_2 are parallel to another line ℓ_2. Therefore, to construct the reference room, we can arbitrarily choose two values φ_1^0 and φ_2^0 from $[0, 2\pi)$ and K values of the angle $\{\theta_k^0\}_{k=1}^K$ from $[0, \pi)$. Then, we match K_1 values of $\{\theta_k^0\}_{k=1}^{K_1}$ with φ_1^0 and the remaining $K_2 = K - K_1$ values of $\{\theta_k^0\}_{k=K_1+1}^{K_2}$ with φ_2^0. This results in a room with the two sets of walls, where all walls in one set are parallel to a line. We can then solve the system of two equations (80) for φ_1^0 and φ_2^0, to find the values of two parameters (e.g. a and b) and leave the third one (e.g. e) free to generate equivalent rooms.

2) *Equivalent room:* We find the equivalent rooms from (67) by the same computations as in Section V-D.

4) *Configurations with the same PPDMs:* A set of room–trajectory configurations with the same PPDMs also corresponds to the one in Section V-D with $c = 0, f = 0$ and $i = \pm 1$. The free parameter e generates equivalent room–trajectory configurations,

$$\begin{aligned}
&\left[\mathcal{R}^0\right] = \left\{\mathcal{R} \,\middle|\, \varphi_k = g(\theta_k^0, \varphi_k^0, s_k, a, b, c = 0, e, f = 0),\right.\\
&\theta_k = f(\theta_k^0, t_k, i = \pm 1),\\
&t_k, s_k \in \{0, 1\} \text{ s.t. } (67) \text{ satisfied},\\
&a \in \mathbb{R} \setminus \{0\}, b \in \mathbb{R}, e \in \mathbb{R} \setminus \{0\} \text{ s.t. } (69) \text{ satisfied},\\
&a \in \mathbb{R} \setminus \{0\}, b \in \mathbb{R} \text{ s.t. } (80) \text{ satisfied}, e \in \mathbb{R}\setminus\{0\},\\
&q_k = q_k^0, \text{ for } 1 \leq k \leq K,\\
&\left.\mathbf{r}_n \text{ s.t. } (77) \text{ satisfied for } 1 \leq n \leq N\right\},
\end{aligned} \tag{83}$$

where the waypoints in the reference room are chosen arbitrarily, while the reference room is constructed from two sets of walls, with walls within each set being parallel to a line.

Note that the walls computed from z_1 do not have to enclose any specific shape, as long as they are equally inclined to all the walls obtained from z_2.

An interesting realistic room that belongs to this case is a room made up of four parallel walls that are perpendicular to the ceiling and the floor. By tilting the ceiling and the floor (changing the value of a), we can generate infinitely many equivalent rooms with respect to PPDM, see Fig. 12.

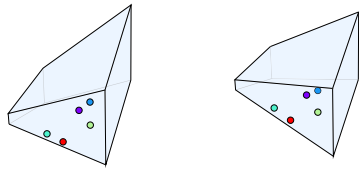

Fig. 12. Equivalent rooms with two groups of walls enclosing a prismatic surface.

F. 3D Rank-4: Planar Trajectories

1) *Linear dependence:* To achieve $\operatorname{rank}(\bar{\mathbf{N}}) = 4$, we assume that the fourth and the fifth column of $\bar{\mathbf{N}}$ are linear combinations of the remaining four,

$$\begin{bmatrix}\sin\theta_k\cos\varphi_k\\ \sin\theta_k\sin\varphi_k\end{bmatrix} = \mathbf{T}\begin{bmatrix}\sin\theta_k^0\cos\varphi_k^0\\ \sin\theta_k^0\sin\varphi_k^0\\ \cos\theta_k^0\\ \cos\theta_k\end{bmatrix}, \tag{84}$$

where

$$\mathbf{T} = \begin{bmatrix}a & b & c & d\\ e & f & g & h\end{bmatrix}. \tag{85}$$

2) *Reparametrization:* As $r > m$, we cannot rewrite (84) so that the normals of $\mathcal{R}$ and $\mathcal{R}^0$ are on different sides.

3) *Reference room:* In (84) we have two equations with four unknown angles for every k. Since the system is underdetermined, we can choose $\{\theta_k^0, \varphi_k^0\}_{k=1}^K$ arbitrarily.

4) *Equivalent rooms:* We solve (84) for θ_k and φ_k, and express their dependence on θ_k^0, φ_k^0 and the parameters in $\mathbf{T}$,

$$\theta_k = s_k f(\theta_k^0, \varphi_k^0, \mathbf{T}), \quad \varphi_k = t_k h(\theta_k^0, \varphi_k^0, \theta_k, \mathbf{T}), \tag{86}$$

where $s_k, t_k \in \{-1, 1\}$, and

$$f(\theta_k^0, \varphi_k^0, \mathbf{T}) = \operatorname{acos} \frac{-dG_a - hG_e \pm \sqrt{G}}{1 + d^2 + h^2},$$
$$h(\theta_k^0, \varphi_k^0, \theta_k, \mathbf{T}) = \operatorname{acos} \frac{d\cos\theta_k + G_a}{\sin\theta_k}, \tag{87}$$

and we introduced the following shortcuts:

$$G_a := a\sin\theta_k^0\cos\varphi_k^0 + b\sin\theta_k^0\sin\varphi_k^0 + c\cos\theta_k^0,$$
$$G_e := e\sin\theta_k^0\cos\varphi_k^0 + f\sin\theta_k^0\sin\varphi_k^0 + g\cos\theta_k^0,$$
$$G := (dG_a + hG_e)^2 - (1 + d^2 + h^2)(G_a^2 + G_e^2 - 1). \tag{88}$$

Moreover, we assume that the parameters in $\mathbf{T}$ are such that

$$|\, -dG_a - hG_e \pm \sqrt{G}\,| \le 1 + d^2 + h^2 \quad \text{and}$$
$$|\, d\cos\theta_k + G_a\,| \le |\sin\theta_k\,|, \tag{89}$$

is satisfied for every triple $(\varphi_k^0, \theta_k^0, \theta_k)$, $1 \le k \le K$.

5) *Corresponding trajectories:* The nullspace of $\bar{\mathbf{N}}^\top$ is spanned by two vectors,

$$\mathbf{v}_1 = \begin{bmatrix} -a, & -b, & -c, & 1, & 0, & -d \end{bmatrix}^\top,$$
$$\mathbf{v}_2 = \begin{bmatrix} -e, & -f, & -g, & 0, & 1, & -h \end{bmatrix}^\top,$$

so the nth row of $\bar{\mathbf{R}}$ is

$$\begin{bmatrix} \mathbf{r}_n^0 \\ -\mathbf{r}_n \end{bmatrix} = \mathbf{v}_1\gamma_1 + \mathbf{v}_2\gamma_2, \tag{90}$$

where $\gamma_1, \gamma_2 \in \mathbb{R}$. From (90) we have that one coordinate of the waypoints $\mathbf{r}_n^0$ and $\mathbf{r}_n$ is a linear combination of the remaining two, meaning that the waypoints lie in a plane. We can for instance choose x and y coordinates of $\mathbf{r}_n^0$ arbitrarily and find $r_{n,z}^0$ from:

$$r_{n,z}^0 = \frac{cf - bg}{af - be} r_{n,x}^0 + \frac{ag - ce}{af - be} r_{n,y}^0.$$

The waypoints in the equivalent room–trajectory configuration are then given by:

$$r_{n,x} = \frac{1}{af - be}(f r_{n,x}^0 - e r_{n,y}^0)$$
$$r_{n,y} = \frac{1}{af - be}(-b r_{n,x}^0 + a r_{n,y}^0)$$
$$r_{n,z} = -d r_{n,x} - h r_{n,y}.$$

For a system to have a solution we assume that $af \neq be$. We could also choose y and z coordinates of $\mathbf{r}_n^0$ arbitrarily, find x as their linear combination and require $bg \neq cf$, or, analogously, we could choose x and z coordinates of $\mathbf{r}_n^0$ arbitrarily, find y as their linear combination and assume that $ag \neq ce$.

6) *Configurations with the same PPDMs:* A set of room–trajectory configurations generated by $\mathcal{R}^0$ with an arbitrary room $\{\mathcal{P}_k^0\}_{k=1}^K$ and a planar trajectory $\{\mathbf{r}_n^0\}_{n=1}^N$ is given as:

$$\begin{aligned} &\left[\mathcal{R}^0\right] = \left\{\mathcal{R} \,\middle|\, \theta_k = s_k f(\theta_k^0, \varphi_k^0, \mathbf{T}), \varphi_k = t_k h(\theta_k^0, \varphi_k^0, \mathbf{T}),\right. \\ &a, b, c, d, e, f, g, h \in \mathbb{R} \text{ s.t. } (89) \text{ holds and } (90) \text{ consistent}, \\ &s_k, t_k \in \{0, 1\}, q_k = q_k^0 \text{ for } 1 \le k \le K, \\ &\left.\mathbf{r}_n \text{ s.t. } (90) \text{ satisfied for } 1 \le n \le N\right\}. \end{aligned} \tag{91}$$

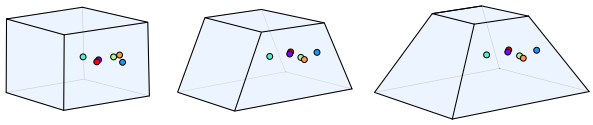

Fig. 13. Rooms with planar trajectories and the same PPDM.

We conclude that for arbitrarily chosen wall normals of the reference room, we can always find another room with identical distance measurements, as long as the trajectories in both rooms are planar, as in Fig. 13.

G. 3D Rank-5: Linear Trajectories

1) *Linear dependence:* Finally, let $\operatorname{rank}(\bar{\mathbf{N}}) = 5$, so that one column of $\bar{\mathbf{N}}^\top$ is a linear combination of the remaining independent columns,

$$\cos\theta_k = \mathbf{T} \begin{bmatrix} \sin\theta_k\cos\varphi_k \\ \sin\theta_k\sin\varphi_k \\ \sin\theta_k^0\cos\varphi_k^0 \\ \sin\theta_k^0\sin\varphi_k^0 \\ \cos\theta_k^0 \end{bmatrix},$$
$$\text{where } \mathbf{T} = \begin{bmatrix} a & b & c & d & e \end{bmatrix}. \tag{92}$$

2) *Reparametrization:* Since $r > m$, this step is a no-op.

3) *Reference room:* From (92), we can choose walls of the reference room arbitrarily.

4) *Equivalent rooms:* Furthermore, we can express θ_k as a function of φ_k, θ_k^0, φ_k^0 and the parameters in $\mathbf{T}$,

$$\theta_k = f(\varphi_k, \theta_k^0, \varphi_k^0, s_k, \mathbf{T}), \tag{93}$$

where

$$h(\varphi_k, a, b) = a\cos\varphi_k + b\sin\varphi_k,$$
$$g(\varphi_k, \theta_k^0, \varphi_k^0, \mathbf{T}) = (\cdots)$$
$$(\cdots) = \operatorname{acos} \frac{d\sin\theta_k^0\sin\varphi_k^0 + e\cos\theta_k^0 + c\sin\theta_k^0\cos\varphi_k^0}{\sqrt{h(a, b, \varphi_k)^2 + 1}},$$
$$f(\varphi_k, \theta_k^0, \varphi_k^0, s_k, \mathbf{T}) = s_k g(\varphi_k, \theta_k^0, \varphi_k^0, \mathbf{T}) - \operatorname{atan} h(\varphi_k, a, b), \tag{94}$$

with $s_k \in \{-1, 1\}$ and

$$|\sin\theta_k^0(d\sin\varphi_k^0 + c\cos\varphi_k^0) + e\cos\theta_k^0\,| \le \sqrt{h(a, b, \varphi_k)^2 + 1}, \tag{95}$$

for every triplet of wall parameters $(\theta_k^0, \varphi_k^0, \varphi_k)$, $1 \le k \le K$.

5) *Corresponding trajectories:* The nullspace of $\bar{\mathbf{N}}^\top$ is spanned by

$$\mathbf{v}_1 = \begin{bmatrix} -c, & -d, & -e, & -a, & -b, & 1 \end{bmatrix}^\top,$$

so the columns of $\bar{\mathbf{R}}$ have to be of the form

$$\begin{bmatrix} \mathbf{r}_n^0 \\ -\mathbf{r}_n \end{bmatrix} = \mathbf{v}_1\gamma, \tag{96}$$

where $\gamma \in \mathbb{R}$. The above equation can be rewritten as $\mathbf{r}_n = \mathbf{S}\mathbf{r}_n^0$, where $\mathbf{S}$ is a scaling matrix with $-\frac{a}{c}$, $-\frac{b}{d}$ and $\frac{1}{e}$ on a diagonal.

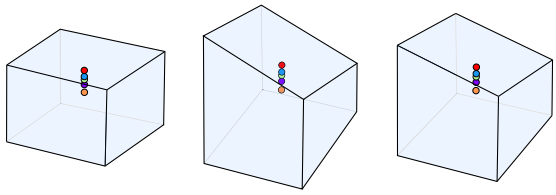

Fig. 14. Rooms with linear trajectories and the same PPDM.

Moreover, x and y coordinates of the waypoints $\{\mathbf{r}_n^0\}_{n=1}^N$ are only scaled values of the z coordinates, so the trajectories are linear. With $c \neq 0, d \neq 0$ and $e \neq 0$ we ensure that the waypoints in the reference room are not restricted to lie on the coordinate axes.

6) *Configurations with the same PPDMs:* A room–trajectory configuration $\mathcal{R}^0$ with arbitrary wall normals $\{\mathcal{P}_k^0\}_{k=1}^K$ and a linear trajectory $\{\mathbf{r}_n^0\}_{n=1}^N$ generates the following set of room–trajectory configurations with the same PPDMs:

$$\begin{aligned}&\left[\mathcal{R}^0\right] = \left\{\mathcal{R} \,\middle|\, \theta_k = f(\varphi_k, \theta_k^0, \varphi_k^0, s_k, \mathbf{T}), \varphi_k \in [0, 2\pi\},\right.\\ &a, b \in \mathbb{R}, c, d, e \in \mathbb{R}\backslash\{0\} \text{ s.t. } (95) \text{ satisfied},\\ &s_k \in \{-1, 1\}, q_k = q_k^0, \text{ for } 1 \leq k \leq K,\\ &\left.\mathbf{r}_n \text{ s.t. } (96) \text{ satisfied for } 1 \leq n \leq N\right\}. \end{aligned} \tag{97}$$

We conclude that for any arbitrarily chosen room, we can always find another room with the same PPDM, as long as the trajectories in both rooms are linear. While linear trajectories may seem a special case of the previous one, the room transformations are rather different. One example of such configurations is illustrated in Fig. 14.

VI. Implications for SLAM in Practice

The analysis in Section IV and Section V shows that we cannot always uniquely reconstruct points and planes from their pairwise distances. In practice, this indicates that solving the problem of simultaneous localization and mapping with a mobile device that measures its distance from the walls of a room does not have a unique solution in all environments. Here we discuss two directions to reduce the solution space: by adding constraints on the room geometry or by adding constraints on the trajectory of the device.

A. Constraints on Room Geometries

As shown in the analysis, linear and planar trajectories introduce additional ambiguities in the room reconstruction, so one should avoid them. Let us thus assume in this discussion that a trajectory is non-linear in 2D and non-planar in 3D, and provide an overview of rooms that cannot be uniquely reconstructed from the distance measurements.

In 2D, this concerns only parallelogram rooms. We showed in Section IV-A that they have one degree of freedom to generate new rooms within the set of room–trajectory configurations with the same PPDMs. Hence, if one knows that the reconstruction takes places in a rectangular room, it is sufficient to fix one angle of the room to be the right angle and obtain a unique reconstruction and localization.

In 3D, rooms from Section V-B are not uniquely determined by the distance measurements; we call them parallelepipeds without bases. It is clear that in reality "rooms" without ceiling and floor are not common, but it can happen that the ceiling and the floor are covered by materials that are not reflective (for example, metal mesh system for the ceiling and carpets on the floor), so that the device cannot measure its distance from the ceiling and the floor by radio or sound waves. Similar to parallelograms, we showed that the rooms from the set of room–trajectory configurations with the same PPDMs can be generated by changing one degree of freedom, and thus, if one knows that the reconstruction takes places in a room with a rectangular floor plan, it is sufficient to fix one angle of the room to be the right angle and obtain a unique reconstruction and localization.

A similar argument is valid for the rooms from Section V-E that can be constructed from two independent sets of walls, where all walls within a set are parallel to a line. If one set is floor and ceiling and the other comprises side walls, we get familiar, realistic rooms. If one knows that the floor is perpendicular to the side walls, it is sufficient to fix the angle between two sets of walls to be the right angle to get uniqueness.

It is not possible to identify uniqueness conditions for the rooms in Section V-D, but they can be constrained using trajectory information discussed in Section VI-B.

In conclusion, most rooms we know from daily life belong to one of the three cases mentioned above: parallelograms, parallelepipeds without bases, and two sets of walls parallel to a line. For these rooms, uniqueness is guaranteed already if we fix one degree of freedom, for example one angle.

B. Constraints on Trajectories

In addition to constraining rooms, it might be natural to constrain trajectories. In practice, various techniques can be used to get a noisy estimate of the motion of the device, such as odometry, and acquire some knowledge about the trajectories. If this information was noiseless and the trajectories were non-planar, we could uniquely reconstruct all rooms from the distance measurements and known trajectories [36]. Even when noisy, these additional measurements constrain the plausible reconstructions to a neighborhood of the correct one in the room–trajectory space. This is illustrated in Fig. 15, with the reconstruction algorithm explained in Section VII.

VII. Reconstruction Algorithm and Experimental Results

In this section, we study how room–trajectory configurations can be reconstructed from PPDMs. In the noiseless case, a room–trajectory configuration can be recovered from only a few distance measurements by solving the polynomial equations (4), at least in principle. In practice, however, polynomial solvers are brittle in the presence of noise. Additionally, this algebraic approach makes it difficult to incorporate prior knowledge we might have about the room or the trajectory.

We therefore formulate the joint recovery as an optimization problem and aim to estimate a room–trajectory configuration that best fits the given measured distances. More precisely, we formulate the problem as a low-rank matrix factorization: given noisy and incomplete PPDM $\widetilde{\mathbf{D}}$, we want to jointly recover the waypoints $\hat{\mathbf{R}}$, the wall normals in a column-unitary matrix $\hat{\mathbf{N}}$

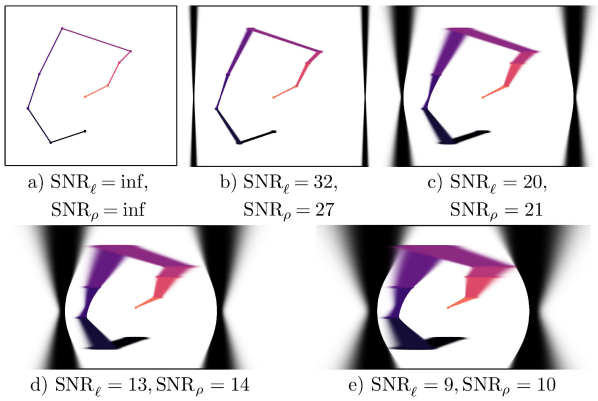

Fig. 15. Room–trajectory configurations equivalent to a rectangular room for different noise levels in the motion model. We consider independent Gaussian noise on the length and angle of the vectors between two waypoints. The noiseless case in a) shows that there is only one room–trajectory configuration for the given PPDM and the noiseless measurement of the trajectory. The more noise we assume in the motion model, the more room–trajectory configurations become feasible. Different values of signal-to-noise ratio (SNR) of lengths and angles are illustrated from b) to e). The opacity of the rooms and trajectories is proportional to the probability of their realization. All values are in decibels.

and the distances of the walls from the origin $\hat{\mathbf{q}}$, such that

$$\hat{\mathbf{R}}, \hat{\mathbf{N}}, \hat{\mathbf{q}} = \underset{\mathbf{R},\mathbf{N},\mathbf{q}}{\operatorname{argmin}} \left\| \widetilde{\mathbf{D}} - \mathbf{W} \circ \left(\mathbf{1}\mathbf{q}^\top - \mathbf{R}^\top \mathbf{N} \right) \right\|^2. \tag{98}$$

A binary mask $\mathbf{W} \in \mathbb{R}^{N \times K}$ is one at positions of measured entries and zero otherwise, so that the noisy and incomplete $\widetilde{\mathbf{D}}$ is defined as $\widetilde{\mathbf{D}} = \mathbf{W} \circ (\mathbf{D} + \mathbf{Z})$. We assume that $\mathbf{Z} \in \mathbb{R}^{N \times K}$ is iid noise; $\circ$ is the Hadamard product.

The formulation (98) is not novel; for instance, it has been used to solve the problem of localizing a set of microphones and a set of acoustic sources from sound propagation times [1], [35]. The authors propose to reduce (4) to

$$\mathbf{D}' = -\mathbf{R}'^\top \mathbf{N} \tag{99}$$

at the expense of losing one measurement. To that end, they translate the waypoints $\mathbf{R}$ such that the ith waypoint is at the origin and delete the ith column of the translated $\mathbf{R}$ to obtain $\mathbf{R}' \in \mathbb{R}^{m \times (N-1)}$. The distance between the translated $\mathbf{r}_i$ and the translated kth wall is equal to q_k; hence, $\mathbf{1}\mathbf{q}^\top$ is eliminated by subtracting the ith row of $\mathbf{D}$ from all rows in $\mathbf{D}$. Lastly, $\mathbf{D}' \in \mathbb{R}^{(N-1) \times K}$ is computed by deleting the ith row of this translated $\mathbf{D}$. The factorization of $\mathbf{D}'$ then jointly recovers the $N-1$ non-zero waypoints in $\mathbf{R}'$ and the K wall normals in $\mathbf{N}$.

In the presence of noise and missing measurements, we obtain a noisy and incomplete $\widetilde{\mathbf{D}}'$, such that a factorization solve (99) might not exist. Thus, we aim to recover $\mathbf{R}$ and $\mathbf{N}$ by solving the following minimization problem:

$$\hat{\mathbf{R}}, \hat{\mathbf{N}} = \underset{\mathbf{R}, \mathbf{N}}{\operatorname{argmin}} \left\| \widetilde{\mathbf{D}}' + \mathbf{W}' \circ (\mathbf{R}'^\top \mathbf{N}) \right\|^2, \tag{100}$$

where $\mathbf{W}'$ is computed from $\mathbf{W}$ by removing the ith row.

While the cost function in (100) is not convex, there are a number of techniques that find local minima; empirically, they in fact find global minima. We use the alternating optimization (AO) algorithm [35] because it works with an incomplete PPDM as long as the matrix contains at least one complete row. The algorithm alternates between estimates $\hat{\mathbf{R}}'_\ell$ and $\hat{\mathbf{N}}_\ell$, and at each

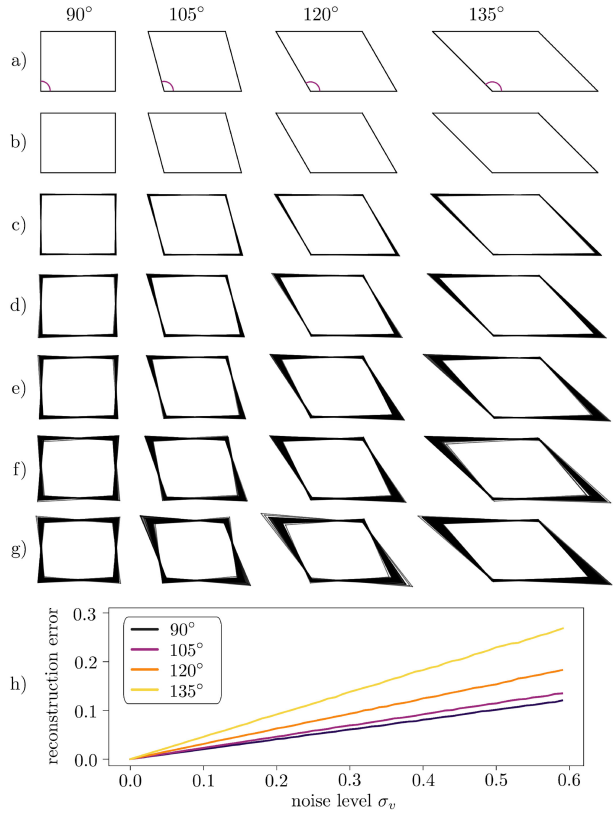

Fig. 16. Example of four rooms with the same PPDM, whose noisy normals are used as initial values of the AO algorithm. a) Original rooms. b)–g) Rooms reconstructed by the AO algorithm. Initial values $\hat{\mathbf{N}}_0$ are created by adding independent Gaussian noise $\mathcal{N}(0, \sigma_v^2 \mathbf{I})$ to the vertices of the original rooms, where σ_v is equal to b) 0, c) 0.1, d) 0.2, e) 0.3, f) 0.4, g) 0.5. h) Dependence of the reconstruction error on $\hat{\mathbf{N}}_0$.

step $\ell = 0, 1, 2, \ldots$ finds the optimal $\hat{\mathbf{N}}_\ell$ for a fixed $\hat{\mathbf{R}}'_{\ell-1}$, and analogously, the optimal $\hat{\mathbf{R}}'_\ell$ for a fixed $\hat{\mathbf{N}}_{\ell-1}$. We use $\hat{\mathbf{N}}_0$ to denote the initial value of the wall normals and always start by computing $\hat{\mathbf{R}}_1$ given $\hat{\mathbf{N}}_0$ and $\widetilde{\mathbf{D}}'$. This procedure is known to be locally convergent [44].

In the following we evaluate the performacne of the AO algorithm on different room geometries. We focus in particular on configurations which, according to our analysis, are not uniquelly specified by the PPDM measurements. We study how the existence of multiple plausible rooms affects the reconstruction performance.

A. Dependence on Initial Values

We consider different parallelograms with the same PPDMs, four of which are illustrated in Fig. 16a. We randomly generate $N = 10$ waypoints inside each room and compute the corresponding PPDM $\mathbf{D}'$.

To evaluate the dependence of the room reconstruction on the initial value of wall normals, $\hat{\mathbf{N}}_0$, we perform the following steps: We add independent Gaussian noise $\mathcal{N}(\mathbf{0}, \sigma_v^2 \mathbf{I})$ to the vertices of the original rooms. Then, we compute the wall normals $\hat{\mathbf{N}}_0$ from the noisy vertices and use them to initialize the AO algorithm. Clearly, when $\sigma_v = 0$, the algorithm converges after 1 step and the recovered rooms are identical to the original rooms (see Fig. 16b). For $\sigma_v > 0$, the algorithm converges to the parallelogram near the initial $\hat{\mathbf{N}}_0$ among the parallelograms

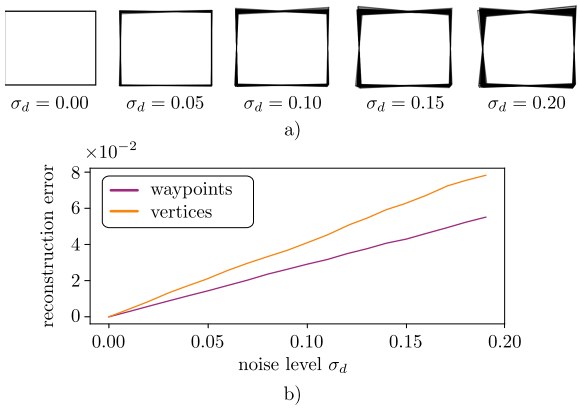

Fig. 17. Extension of the AO algorithm which in every iteration enforces one angle of a room to be right. a) Several rooms reconstructed by the extended AO algorithm. Initial values $\hat{\mathbf{N}}_0$ are chosen randomly, while $\widetilde{\mathbf{D}}'$ is created by adding independent Gaussian noise $\mathcal{N}(0, \sigma_d^2)$ to the entries of $\mathbf{D}'$. b) Dependence of the reconstruction error on σ_d.

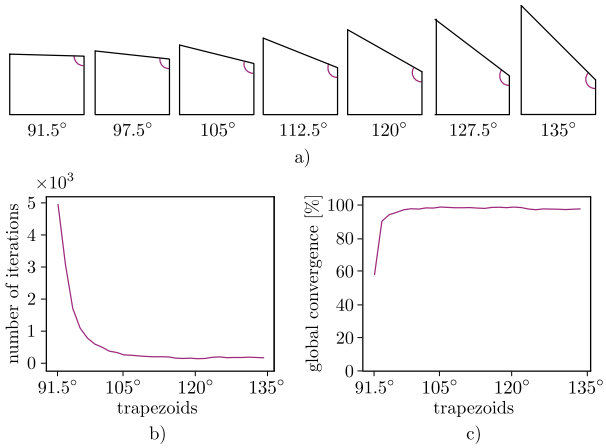

Fig. 18. Performance of the AO algorithm. a) Example of seven different room geometries used to assess the convergence of the AO algorithm. The rooms are the right trapezoids, whose obtuse angles range between 91.5° and 135°. b) Dependence of the average number of iterations performed by the algorithm before it stops (either converges to the optimal solution or exceeds 5000 iterations) on the room geometry. c) Dependence of the percentage of random initializations that converge to the optimal solution on the room geometry.

with the same PPDM (see Fig. 16c to Fig. 16g). For each of the four rooms, we plot in Fig. 16h the reconstruction error, which we define as the average ℓ^2-norm between the reconstructed and the original vertices, after alignment. Observe that since the entries of $\mathbf{D}'$ are noiseless, the cost function (100) always converges to zero, and the value of the reconstruction error depends exclusively on the initial guess of $\hat{\mathbf{N}}_0$.

We conclude that the wall normals $\hat{\mathbf{N}}_0$ used to initialize the AO algorithm have a significant impact on selecting a room from the set of rooms with the same PPDM. This property has two antagonistic effects on the reconstruction. On the one hand, if we have some prior knowledge about the room and our initial guess of $\hat{\mathbf{N}}_0$ is not far from the original wall normals, then the AO algorithm converges to the neighborhood of the original room. On the other hand, if we do not have any prior knowledge about the room and we initialize $\hat{\mathbf{N}}_0$ arbitrarily, the AO algorithm will converge locally to the parallelogram which is the nearest to the initial normals $\hat{\mathbf{N}}_0$.

B. Enforcing a Right Angle

In this section we consider rectangular rooms. The goal is to show that by fixing one angle of a room to be the right angle, and by enforcing this property in every iteration of the AO algorithm, we can navigate to the desired global optimum—a rectangular room. Moreover, we test the robustness of the algorithm to noise.

We perform the following experiment: In a rectangular room, we randomly generate $N = 10$ waypoints and compute a PPDM $\mathbf{D}'$. We then create $\widetilde{\mathbf{D}}'$ by adding independent Gaussian noise $\mathcal{N}(0, \sigma_d^2)$ to the entries of $\mathbf{D}'$. Given $\widetilde{\mathbf{D}}'$ and arbitrarily chosen initial values $\hat{\mathbf{N}}_0$, we run the extended AO algorithm: in every iteration ℓ, the algorithm first finds $\hat{\mathbf{N}}_\ell$ by minimizing (100) for a fixed $\hat{\mathbf{R}}'_{\ell-1}$, and then rotates the first wall of the room to be perpendicular to the second wall.

We present the results of our experiment repeated 1000 times in Fig. 17. It shows that for $\sigma_d = 0$, AO always converges to the global minimum, so the output of the algorithm is the original rectangular room. With $\sigma_d > 0$, we confirm that the algorithm is stable and robust to noise: the average ℓ^2-norm between the original and the reconstructed waypoints, as well as the average ℓ^2-norm between the original and the reconstructed vertices, increases linearly with σ_d (see Fig. 17b). This confirms that the reconstruction error is only due to noisy PPDM measurements (as opposed to optimization artifacts).

C. Dependence on the Room Geometry

We now return to the noiseless setting to study convergence as a function of the room geometry. In particular, we study rooms that are close in shape to parallelograms.

Results of Section VII-A suggests that for parallelograms the cost function (100) has many (near-)global minima, each of corresponding to a distinct parallelogram. This is a pleasing verification of our theoretical results. On the other hand, we know from Section IV that rooms other than parallelograms have a unique PPDM, and therefore, their PPDMs have a unique factorization. In the following experiment, we study the behavior of the AO algorithm in the transition between these two specific classes of rooms, i.e., we focus on rooms that are close in shape to parallelograms.

We create trapezoidal rooms whose three walls correspond to three sides of a rectangle. The angle of the fourth wall is a free variable; in our experiment, it varies from 90° to 135°. Several examples of such rooms are shown in Fig. 18a. For each of these trapezoids, we randomly generate $N = 10$ waypoints, compute a PPDM $\mathbf{D}'$ and run AO with 1000 random initializations. The algorithm stops either if the value of the cost function is smaller than than a prescribed threshold (10^{-5}) or the number of iterations exceeds 5000. In Fig. 18b we plot the average number of iterations performed by the algorithm for different trapezoids, while Fig. 18c plots the percentage of random initializations that converge to the optimal solution.

Our simulations show that the AO algorithm correctly recovers trapezoidal rooms with two right angles and one obtuse angle larger than 105° for 97% of random initialization. Moreover, it takes on average 200 iterations to converge. By narrowing the obtuse angle to $90^\circ + \epsilon$, where $\epsilon > 0$, the percentage of recovering the optimal solution falls to 60%, while the convergence significantly slows down.

We have thus shown that configurations that are in some sense close to those where uniqueness fails lead to sensitive reconstructions. This result is in agreement with intuition. It suggests that in these cases stronger regularization is required, for example by introducing adequate geometric prior knowledge.

VIII. Conclusion

We derived sufficient and necessary conditions for unique reconstruction of points–planes configurations from their pairwise distances. Our analysis hinges on a new algebraic tool called point-to-plane distance matrix. We exhaustively identify the geometries of points and planes that cannot be distinguished given their PPDMs.

Our motivation comes from the challenging problem of multipath-based simultaneous localization and mapping and our study has consequences for practical indoor localization problems. Picture an unknown room with no preinstalled infrastructure and a mobile device equipped with a single omnidirectional source and a single omnidirectional receiver. The distance measurements between the points and planes are given as the time-of-flights of the first-order echoes recorded by the device. Therefore, our theoretical results provide a fundamental understanding and constraints under which rooms can uniquely be reconstructed from only first-order echoes.

Computer experiments in Sections VI and VII present the practical implications of the theoretical results. They show how configurations which are "almost non-unique" lead to poor reconstructions, and how the reconstruction quality can be improved by introducing priors.

While our analysis here starts with the PPDM, preparing the PPDM in real scenarios puts forward additional challenges, namely PPDM completion and denoising, and echo sorting in the acoustic case. Our ongoing research includes the development and implementation of computational tools and heuristics for localization from noisy, incomplete, and unlabeled PPDMs.

Appendix

For all m and r we worked with a particular selection of r independent columns. We prove here that this choice can be made without loss of generality. We will call the particular column choice in Sections IV and V *the original choice*.

First note that there is symmetry between reference and equivalent rooms. For example, for $r = 1$ in 2D, given the original choice of r independent columns we have

$$\left[\sin\varphi_k, \cos\varphi_k^0, \sin\varphi_k^0\right]^\top = \left[a, b, c\right]^\top \cos\varphi_k. \tag{101}$$

We can swap the normals $\{\varphi_k^0\}_{k=1}^K$ and $\{\varphi_k\}_{k=1}^K$ for every k, and obtain a new, symmetric choice of r independent columns

$$\left[\sin\varphi_k^0, \cos\varphi_k, \sin\varphi_k\right]^\top = \left[a, b, c\right]^\top \cos\varphi_k^0. \tag{102}$$

The two systems (101) and (102) result in the same sets of room–trajectory configurations.

A similar conclusion follows if the new choice is obtained by rearranging the order of the coordinates of the normals. Again, for $r = 1$ in 2D we have that

$$\left[\cos\varphi_k^0, \cos\varphi_k, \sin\varphi_k\right]^\top = \left[a, b, c\right]^\top \sin\varphi_k^0 \tag{103}$$

can be transformed to the studied case of (26). Indeed, by applying a rotation by $\pi/2$ to the normals of the reference room, we obtain a new reference room which satisfies (26), but rotated configurations are considered to be equivalent.

In the following we show that any choice of r independent columns not covered by the two previous examples can be transformed into one of the cases analyzed in Sections IV and V (for $r = 2$ in 2D and $r \in \{2, 3, 4\}$ in 3D).

1) **2D rank-2:** By symmetry, it is sufficient to show that

$$\begin{bmatrix}\cos\varphi_k \\ \cos\varphi_k^0\end{bmatrix} = \begin{bmatrix}a & b \\ c & d\end{bmatrix}\begin{bmatrix}\sin\varphi_k \\ \sin\varphi_k^0\end{bmatrix} \tag{104}$$

can be transformed into (14). For $c \neq 0$, it follows directly:

$$\begin{bmatrix}\cos\varphi_k \\ \sin\varphi_k\end{bmatrix} = \frac{1}{c}\begin{bmatrix}a & bc-ad \\ 1 & -d\end{bmatrix}\begin{bmatrix}\cos\varphi_k^0 \\ \sin\varphi_k^0\end{bmatrix}. \tag{105}$$

For $c = 0$ we have $\tan\varphi_k^0 = \frac{1}{d}$, addressed in (26).

2) **3D rank-2:** By symmetry, we only analyze

$$\begin{bmatrix}\cos\theta_k^0 \\ \sin\theta_k^0\sin\varphi_k^0 \\ \sin\theta_k\sin\varphi_k \\ \cos\theta_k\end{bmatrix} = \begin{bmatrix}a & b \\ c & d \\ e & f \\ g & h\end{bmatrix}\begin{bmatrix}\sin\theta_k^0\cos\varphi_k^0 \\ \sin\theta_k\cos\varphi_k\end{bmatrix} \tag{106}$$

and transform it into (49) as

$$\begin{bmatrix}\cos\theta_k^0 \\ \sin\theta_k\cos\varphi_k \\ \sin\theta_k\sin\varphi_k \\ \cos\theta_k\end{bmatrix} = \frac{1}{d}\begin{bmatrix}ad-bc & b \\ -c & 1 \\ ef-cf & f \\ gd-ch & h\end{bmatrix}\begin{bmatrix}\sin\theta_k^0\cos\varphi_k^0 \\ \sin\theta_k^0\sin\varphi_k^0\end{bmatrix} \tag{107}$$

for $d \neq 0$. If $d = 0$ and $b \neq 0$, a substitution $\sin\theta_k\cos\varphi_k = \frac{1}{b}(\cos\theta_k^0 - a\sin\theta_k^0\cos\theta_k^0)$ from the first equation of (106) into the last two equations of (106) gives a system equivalent to (49). For $b = d = 0$, we get constant normals, discussed in (41).

3) **3D rank-3:** Again, we only analyze

$$\begin{bmatrix}\sin\theta_k\cos\varphi_k \\ \sin\theta_k\sin\varphi_k \\ \cos\theta_k^0\end{bmatrix} = \begin{bmatrix}a & b & c \\ d & e & f \\ g & h & i\end{bmatrix}\begin{bmatrix}\sin\theta_k^0\cos\varphi_k^0 \\ \sin\theta_k^0\sin\varphi_k^0 \\ \cos\theta_k\end{bmatrix} \tag{108}$$

and show that we can transform it into (67). Indeed, for $i \neq 0$,

$$\begin{bmatrix}\sin\theta_k\cos\varphi_k \\ \sin\theta_k\sin\varphi_k\end{bmatrix} = \frac{1}{i}\begin{bmatrix}ai-cg & bi-ch & c \\ di-fg & ei-fh & f \\ -g & -h & 1\end{bmatrix} \times \begin{bmatrix}\sin\theta_k^0\cos\varphi_k^0 \\ \sin\theta_k^0\sin\varphi_k^0 \\ \cos\theta_k^0\end{bmatrix}. \tag{109}$$

For $i = 0, g \neq 0$ or $i = g = 0, h \neq 0$ we can substitute either $\sin\theta_k^0\cos\varphi_k^0$ or $\sin\theta_k^0\sin\varphi_k^0$ from the last equation of (108) into the first two equations of (108), getting (84).

The same holds for $i = g = h = 0$, with an additional constraint $\cos\theta_k^0 = 0$ on the reference normals.

4) **3D rank-4:** Let us assume

$$\begin{bmatrix} \sin\theta_k \cos\varphi_k \\ \sin\theta_k^0 \cos\varphi_k^0 \end{bmatrix} = \begin{bmatrix} a & b & c & d \\ e & f & g & h \end{bmatrix} \begin{bmatrix} \sin\theta_k \cos\varphi_k \\ \sin\theta_k^0 \sin\varphi_k^0 \\ \cos\theta_k^0 \\ \cos\theta_k \end{bmatrix}. \quad (110)$$

Thanks to symmetry, this is the only case of our interest and we transform it to the well-studied system (84) for $e \neq 0$:

$$\begin{bmatrix} \sin\theta_k \cos\varphi_k \\ \sin\theta_k \sin\varphi_k \end{bmatrix} = \frac{1}{e} \begin{bmatrix} a & 1 \\ be - af & -f \\ ce - ag & -g \\ de - ah & -h \end{bmatrix}^\top \begin{bmatrix} \sin\theta_k^0 \cos\varphi_k^0 \\ \sin\theta_k^0 \sin\varphi_k^0 \\ \cos\theta_k^0 \\ \cos\theta_k \end{bmatrix}.$$

If $e = 0$ and $h \neq 0$, substituting $\cos\theta_k$ from the second into the first equation of (110) gives (84). By similar substitutions for $e = h = 0$, $f \neq 0$, and $e = f = h = 0$, $g \neq 0$, we get (92). Finally, $e = f = h = g = 0$ also corresponds to $r = 5$ in 3D, with an additional constraint $\sin\theta_k^0 \cos\varphi_k^0 = 0$.

ACKNOWLEDGMENT

The authors would like to thank Prof. Mireille Boutin for helping simplify the proof of Lemma 1.

REFERENCES

[1] S. Thrun, "Affine structure from sound," *Advances Neural Inf. Process. Syst.*, 2006, pp. 1353–1360.
[2] I. Dokmanić, R. Parhizkar, J. Ranieri, and M. Vetterli, "Euclidean distance matrices: Essential theory, algorithms, and applications," *IEEE Signal Process. Mag.*, vol. 32, no. 6, pp. 12–30, Nov. 2015.
[3] P. H. Schönemann, "On metric multidimensional unfolding," *Psychometrika*, vol. 35, no. 3, pp. 349–366, 1970.
[4] S. Bancroft, "An algebraic solution of the GPS equations," *IEEE Trans. Aerosp. Electron. Syst.*, vol. AES-21, no. 1, pp. 56–59, Jan. 1985.
[5] E. Leitinger, F. Meyer, P. Meissner, K. Witrisal, and F. Hlawatsch, "Belief propagation based joint probabilistic data association for multipath-assisted indoor navigation and tracking," in *Proc. Int. Conf. Localization GNSS*, 2016, pp. 1–6.
[6] I. Dokmanić, "Listening to distances and hearing shapes: Inverse problems in room acoustics and beyond," Ph.D. dissertation, School Comput. Commun. Sci., Ecole Polytechnique Fédérale de Lausanne (EPFL), Lausanne, Switzerland, 2015.
[7] I. Dokmanić, R. Parhizkar, A. Walther, Y. M. Lu, and M. Vetterli, "Acoustic echoes reveal room shape," *Proc. Nat. Acad. Sci.*, vol. 110, no. 30, pp. 12 186–12 191, 2013.
[8] F. Antonacci *et al.*, "Inference of room geometry from acoustic impulse responses," *IEEE Trans. Audio, Speech, Lang. Process.*, vol. 20, no. 10, pp. 2683–2695, Dec. 2012.
[9] C. Brunner, T. Peynot, and T. Vidal-Calleja, "Combining multiple sensor modalities for a localisation robust to smoke," in *Proc. IEEE/RSJ Int. Conf. Intell. Robots Syst.*, 2011, pp. 2489–2496.
[10] V. Kubelka, L. Oswald, F. Pomerleau, F. Colas, T. Svoboda, and M. Reinstein, "Robust data fusion of multimodal sensory information for mobile robots," *J. Field Robot.*, vol. 32, no. 4, pp. 447–473, 2015.
[11] M. Milford, A. Jacobson, Z. Chen, and G. Wyeth, "RatSLAM: Using models of rodent hippocampus for robot navigation and beyond," in *Robotics Research*. Berlin, Germany: Springer, 2016, pp. 467–485.
[12] J. Edwards, "Signal processing improves autonomous vehicle navigation accuracy: Guidance innovations promise safer and more reliable autonomous vehicle operation [special reports]," *IEEE Signal Process. Mag.*, vol. 36, no. 2, pp. 15–18, Mar. 2019.
[13] H. Kim and M. Viberg, "Two decades of array signal processing research," *IEEE Signal Process. Mag.*, vol. 13, no. 4, pp. 67–94, Jul. 1996.
[14] S. Patole and M. Torlak, "Two dimensional array imaging with beam steered data," *IEEE Trans. Image Process.*, vol. 22, no. 12, pp. 5181–5189, Dec. 2013.
[15] J.-S. Hu, C.-Y. Chan, C.-K. Wang, M.-T. Lee, and C.-Y. Kuo, "Simultaneous localization of a mobile robot and multiple sound sources using a microphone array," *Adv. Robot.*, vol. 25, no. 1-2, pp. 135–152, 2011.
[16] C. Evers, A. H. Moore, and P. A. Naylor, "Acoustic simultaneous localization and mapping (a-SLAM) of a moving microphone array and its surrounding speakers," in *Proc. IEEE Int. Conf. Acoust., Speech Signal Process.*, 2016, pp. 6–10.
[17] C. Evers and P. A. Naylor, "Acoustic SLAM," *IEEE/ACM Trans. Audio, Speech, Lang. Process.*, vol. 26, no. 9, pp. 1484–1498, 2018.
[18] J. Kietlinski-Zaleski, "Ultra-wideband positioning using reflections from known indoor features," Ph.D. dissertation, Sch. Eng., Nagoya Univ., Japan, 2011.
[19] J. Kietlinski-Zaleski and T. Yamazato, "TDoA UWB positioning with three receivers using known indoor features," *IEICE Trans. Fundam. Electron., Commun. Comput. Sci.*, vol. 94, no. 3, pp. 964–971, 2011.
[20] P. Meissner, "Multipath-assisted indoor positioning," Ph.D. dissertation, Fac. Elect. Inf. Eng., , Graz Univ. of Technol., Graz, Austria, 2014.
[21] E. Leitinger, P. Meissner, M. Lafer, and K. Witrisal, "Simultaneous localization and mapping using multipath channel information," in *Proc. IEEE Int. Conf. Commun. Workshop*, 2015, pp. 754–760.
[22] I. Dokmanić, L. Daudet, and M. Vetterli, "How to localize ten microphones in one finger snap," in *Proc. 22nd Eur. Signal Process. Conf.*, 2014, pp. 2275–2279.
[23] E. Leitinger, F. Meyer, F. Tufvesson, and K. Witrisal, "Factor graph based simultaneous localization and mapping using multipath channel information," in *Proc. Int. Conf. Commun. Workshops*, Jun. 2017, pp. 652–658.
[24] E. Leitinger, F. Meyer, F. Hlawatsch, K. Witrisal, F. Tufvesson, and M. Z. Win, "A belief propagation algorithm for multipath-based SLAM," *IEEE Trans. Wireless Commun.*, vol. 18, pp. 5613–5629, no. 11, Dec. 2019.
[25] E. Leitinger, S. Grebien, X. Li, F. Tufvesson, and K. Witrisal, "On the use of MPC amplitude information in radio signal based SLAM," in *Proc. Statistical Signal Process. Workshop*, Jun. 2018, pp. 633–637.
[26] E. Leitinger, S. Grebien, and K. Witrisal, "Multipath-based SLAM exploiting AoA and amplitude information," in *Proc. IEEE Int. Conf. Commun. Workshops*, May 2019, pp. 1–7.
[27] O. Shih and A. Rowe, "Can a phone hear the shape of a room?" in *Proc. 18th Int. Conf. Inf. Process. Sensor Netw.* ACM, 2019, pp. 277–288.
[28] B. Zhou, M. Elbadry, R. Gao, and F. Ye, "BatMapper: Acoustic sensing based indoor floor plan construction using smartphones," in *Proc. 15th Annu. Int. Conf. Mobile Syst., Appl., Serv.*, 2017, pp. 42–55.
[29] S. Pradhan, G. Baig, W. Mao, L. Qiu, G. Chen, and B. Yang, "Smartphone-based acoustic indoor space mapping," *Proc. ACM Interactive, Mobile, Wearable Ubiquitous Technol.*, vol. 2, no. 2, 2018, Art. no. 75.
[30] G. Schouten and J. Steckel, "Principles of biological echolocation applied to radar sensing: Applying biomimetic sensors to achieve autonomous navigation," *IEEE Signal Process. Mag.*, vol. 36, no. 4, pp. 98–111, Jul. 2019.
[31] E. Leitinger, P. Meissner, C. Rudisser, G. Dumphart, and K. Witrisal, "Evaluation of position-related information in multipath components for indoor positioning," *IEEE J. Sel. Areas Commun.*, vol. 33, no. 11, pp. 2313–2328, Nov. 2015.
[32] K. Witrisal *et al.*, "High-accuracy localization for assisted living: 5G systems will turn multipath channels from foe to friend," *IEEE Signal Process. Mag.*, vol. 33, no. 2, pp. 59–70, Mar. 2016.
[33] A. Shahmansoori, G. E. Garcia, G. Destino, G. Seco-Granados, and H. Wymeersch, "Position and orientation estimation through millimeter-wave MIMO in 5G systems," *IEEE Trans. Wireless Commun.*, vol. 17, no. 3, pp. 1822–1835, Mar. 2018.
[34] R. Mendrzik, H. Wymeersch, G. Bauch, and Z. Abu-Shaban, "Harnessing NLOS components for position and orientation estimation in 5G millimeter wave MIMO," *IEEE Trans. Wireless Commun.*, vol. 18, no. 1, pp. 93–107, Jan. 2019.
[35] Y. Kuang, E. Ask, S. Burgess, and K. Åström, "Understanding TOA and TDOA network calibration using far field approximation as initial estimate," in *Proc. Int. Conf. Pattern Recognit. Appl. Methods*, 2012, pp. 590–596.
[36] M. Kreković, I. Dokmanić, and M. Vetterli, "EchoSLAM: Simultaneous localization and mapping with acoustic echoes," in *Proc. IEEE Int. Conf. Acoust., Speech Signal Process.*, 2016, pp. 11–15.
[37] M. Kreković, G. Baechler, I. Dokmanić, and M. Vetterli, "Structure from sound with incomplete data," in *Proc. IEEE Int. Conf. Acoust., Speech Signal Process.*, 2018, pp. 3539–3543.

[38] F. Peng, T. Wang, and B. Chen, "Room shape reconstruction with a single mobile acoustic sensor," in *Proc. IEEE Global Conf. Signal Inf. Process.*, 2015, pp. 1116–1120.
[39] M. Boutin and G. Kemper, "A drone can hear the shape of a room," in *SIAM J. Applied Algebra Geometry*, vol. 4, no. 1, 2019, pp. 123–140.
[40] M. Kreković, I. Dokmanić, and M. Vetterli, "Look, no beacons! Optimal all-in-one EchoSLAM," 2016, *arXiv:1608.08753*.
[41] M. Kreković, I. Dokmanić, and M. Vetterli, "Omnidirectional bats, point-to-plane distances, and the price of uniqueness," in *Proc. IEEE Int. Conf. Acoust., Speech Signal Process.*, 2017, pp. 3261–3265.
[42] H. Deusch, S. Reuter, and K. Dietmayer, "The labeled multi-Bernoulli SLAM filter," *IEEE Signal Process. Lett.*, vol. 22, no. 10, pp. 1561–1565, Oct. 2015.
[43] W. Givens, "Computation of plain unitary rotations transforming a general matrix to triangular form," *J. Soc. Ind. Appl. Math.*, vol. 6, no. 1, pp. 26–50, 1958.
[44] J. C. Bezdek, R. J. Hathaway, R. E. Howard, C. A. Wilson, and M. P. Windham, "Local convergence analysis of a grouped variable version of coordinate descent," *J. Optim. Theory Appl.*, vol. 54, no. 3, pp. 471–477, 1987.

Miranda Kreković (Student Member, IEEE) received the B.Sc. degree in computing, information processing, and multimedia systems from the Faculty of Electrical Engineering and Computing, University of Zagreb, Zagreb, Croatia, in 2012 and the the master's degree *(Summa Cum Laude)* in information and communication technology from the same university in 2014. She received the Ph.D. degree in computer and communication sciences from the Audiovisual Communications Laboratory, Ecole Polytechnique Fdrale de Lausanne, Lausanne, Switzerland under the supervision of Prof. Martin Vetterli and Prof. Ivan Dokmanić, in October 2019. From 2010 to 2014, she was a Receiver of the Deans Award "Josip Lončar" for outstanding performance awarded to the top 1% of all students. Her present research mainly addresses simultaneous localization and mapping (SLAM) for an echolocating robot in indoor environments. She studies the question of uniqueness of the room geometry reconstruction from acoustic impulse responses and works on computational tools and algorithms for acoustic SLAM. In fall 2016, she did a research internship at Google Mountain View with Sound Understanding team, where she worked on the blind source separation for simultaneous speech. In summer 2018, she did an internship at Google Zürich with the VideoAds Quality team. Apart from her Ph.D. work, her big passion is to promote computer science and computational thinking to children and teenagers. As a co-founder of *GirlsCoding.org*, she organizes hands-on workshops to motivate girls at the early age to embrace technologies and a possibility of having a career in STEM fields, gives talks to parents and children on related topics, and creates a content for programming courses in private schools. In 2018, she was a finalist of Women Techmakers Scholars Program.

Ivan Dokmanić (Member, IEEE) received the diploma in electrical engineering from the University of Zagreb, Zagreb, Croatia, in 2007 and the doctorate degree in computer and communication science from Ecole Polytechnique Fdrale de Lausanne (EPFL), Lausanne, Switzerland, in 2015. Since 2019, he has been an Associate Professor with the Department of Mathematics and Computer Science, the University of Basel, Switzerland, and since 2016 an Assistant Professor of ECE in the Coordinated Science Laboratory, University of Illinois at Urbana-Champaign, USA (on leave). He has held visiting positions with EPFL (2017, 2018) and ETHZ (2019). From 2015 to 2016, he worked as a Post-Doc with the Institut Langevin and Ecole Normale Suprieure in Paris. During summer 2013, he was with Microsoft Research in Redmond, Washington. Before that he was a Teaching Assistant with the University of Zagreb, a Codec Developer for MainConcept AG, and a Digital Audio Effects Designer for Little Endian Ltd. His research interests lie between data science, physics, and signal processing. For his work on room shape reconstruction using sound, he was the recipient of the Best Student Paper Award at ICASSP 2011; in 2014 he was the recipient of a Google Ph.D. Fellowship. He is a laureate of the EPFL Outstanding Doctoral Thesis Award and the Google Faculty Research Award. In 2019, the European Research Council awarded him a Starting Grant. He used to be the singer and the lead guitarist of Ivan and the Terribles, featuring Martin Vetterli on bass, Paolo Prandoni on everything, and Marta Martinez-Cmara on saxophone.

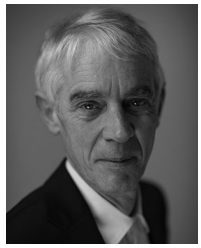

Martin Vetterli (Fellow, IEEE) received the Dipl. El.-Ing. degree from ETH Zurich (ETHZ), Zurich, Switzerland, in 1981, the M.S. degree from Stanford University, Stanford, CA, USA, in 1982, and the Doctorate Sciences degree from Ecole Polytechnique Fdrale de Lausanne (EPFL), Lausanne, Switzerland, in 1986. He was a Research Assistant with Stanford and EPFL, and has worked for Siemens and AT&T Bell Laboratories. In 1986, he joined Columbia University in New York, where he was last an Associate Professor of Electrical Engineering and Co-Director of the Image and Advanced Television Laboratory. In 1993, he joined the University of California at Berkeley, where he was a Professor in the Department of Electrical Engineering and Computer Sciences until 1997, and has held an Adjunct Professor position until June 2010. Since 1995, he has been a Professor of Communication Systems with EPF Lausanne, Switzerland, where he chaired the Communications Systems Division (1996/1997), and heads the Audiovisual Communications Laboratory. From 2001 to 2004, he directed the National Competence Center in Research on mobile information and communication systems. He was also the Vice President with EPFL from October 2004 to February 2011 in charge, among others, of international affairs and computing services. He has held visiting positions with ETHZ (1990) and Stanford (1998). From March 2011 to 2012, he was the Dean of the School of Computer and Communication Sciences of EPFL. From 2013 to 2016, he led the Swiss National Science Foundation and since 2017 he has been the President of EPFL. He has authored about 190 journal papers on a variety of topics in signal/image processing and communications and holds about 50 patents and patent applications. His research interests include sampling, wavelets, multirate signal processing, computational complexity, signal processing for communications, digital image/video processing, joint source/channel coding, signal processing for sensor networks and inverse problems like acoustic tomography. He is a Fellow of ACM, a Fellow of EURASIP, and a member of SIAM and NAE. He is on the editorial boards of *Applied and Computational Harmonic Analysis*, the *Journal of Fourier Analysis and Application,* and the IEEE JOURNAL ON SELECTED TOPICS IN SIGNAL PROCESSING and has been elected Foreign Member of the NAE in 2015. He was the recipient of the Best Paper Award of EURASIP in 1984, the Research Prize of the Brown Bovery Corporation (Switzerland) in 1986, the IEEE Signal Processing Society's Senior Paper Awards in 1991, in 1996 and in 2006 (for papers with D. LeGall, K. Ramchandran, and Marziliano and Blu, respectively). He won the Swiss National Latsis Prize in 1996, the SPIE Presidential award in 1999, the IEEE Signal Processing Technical Achievement Award in 2001, the IEEE Signal Processing Society Award in 2010 for fundamental contributions to signal processing theory, technology and education, and the IEEE Jack S. Kilby Signal Processing Medal in 2017. He is an ISI highly cited Researcher in engineering. He was a member of the Swiss Council on Science and Technology from 2000 to 2003. He was a Plenary Speaker at various conferences (e.g. IEEE ICIP, ICASSP, ISIT) and is the coauthor of three books with J. Kovacevic, "Wavelets and Subband Coding," 1995, with P. Prandoni "Signal Processing for Communications," 2008 and with J. Kovacevic and V.K. Goyal, "Foundations of Signal Processing, 2015.